Spatial Pattern and Zonal Shift of the North Atlantic Oscillation. Part II: Numerical Experiments

DEHAI LUO

Physical Oceanography Laboratory, College of Physical and Environmental Oceanography, Ocean University of China, Qingdao, China

LINHAO ZHONG

LACS, Institute of Atmospheric Physics, Chinese Academy of Sciences, Beijing, China

RONGCAI REN

LASG, Institute of Atmospheric Physics, Chinese Academy of Sciences, Beijing, China

CHUNZAI WANG

NOAA/Atlantic Oceanographic and Meteorological Laboratory, Miami, Florida

(Manuscript received 2 October 2009, in final form 12 April 2010)

ABSTRACT

In this part, the spatial evolution of an initial dipole anomaly in a prescribed jet is at first investigated by numerically solving linear and nonlinear models without forcing in order to examine how the spatial pattern of a dipole anomaly depends on the meridional distribution of a specified jet. It is shown that in a linear experiment an initial symmetric dipole anomaly in the meridional direction can evolve into a northeast–southwest (NE–SW) or northwest–southeast (NW–SE) tilted dipole structure if the core of this jet is in higher latitudes (the north) or in lower latitudes (the south). This is in agreement with the result predicted by the linear Rossby wave theory in slowly varying media. The conclusion also holds for the nonlinear and unforced experiment.

North Atlantic Oscillation (NAO) events are then reproduced in a fully nonlinear barotropic model with a wavemaker that mimics the Atlantic storm-track eddy activity. In the absence of topography the spatial tilting of the eddy-driven NAO pattern is found to be independent of the NAO phase. The eddy-driven NAO pattern for the positive (negative) phase can exhibit a NE–SW (NW–SE) tilting only when the core of a prescribed jet prior to the NAO is confined in the higher latitude (lower latitude) region. However, in the presence of the wavenumber-2 topography (two oceans and continents) in the Northern Hemisphere the spatial tilting of the eddy-driven NAO dipole anomaly can be dependent on the NAO phase. Even when the specified basic flow prior to the NAO is uniform, the eddy-driven positive (negative) NAO phase dipole anomaly can also show a NE–SW (NW–SE) tilting because the northward (southward) shift of the excited westerly jet can occur in the presence of topography. In addition, it is found that when the wavemaker is closer to the position of the initial NAO, the eddy-driven positive (negative) NAO phase pattern can display a whole eastward shift and a more distinct NE–SW (NW–SE) tilting. This thus explains why the first empirical orthogonal function of the NAO pattern observed during 1998–2007 exhibits a more pronounced NE–SW tilting than during 1978–97. It appears that the latitudinal shift of the jet, the large-scale topography, and the zonal position of the Atlantic storm-track eddy activity are three important factors for controlling the spatial tilting and zonal shift of eddy-driven NAO dipole anomalies.

1. Introduction

It has been recognized that the center of action of the North Atlantic Oscillation (NAO) undergoes an eastward shift during the period of 1978–97 (P2) compared

Corresponding author address: Dr. Dehai Luo, College of Physical and Environmental Oceanography, Ocean University of China, Qingdao 266003, China.
E-mail: ldh@ouc.edu.cn

DOI: 10.1175/2010JAS3340.1

to the period of 1958–77 (P1) (Ulbrich and Christoph 1999; Hilmer and Jung 2000; Jung and Hilmer 2001; Jung et al. 2003; Johnson et al. 2008). This eastward shift of the center of action of the NAO pattern is found to result in a prominent difference of the regional climate over the Atlantic and –Europe between P2 and P1 (Jung and Hilmer 2001). Thus, this issue has led to increasing scientific interest since it was detected by Hilmer and Jung (2000).

In a companion paper (Luo et al. 2010, hereafter Part I) we found that the NAO dipole anomaly exhibits a northeast–southwest (NE–SW) tilting for the positive NAO phase and a northwest–southeast (NW–SE) tilting for the negative NAO phase. A new dynamical explanation of the spatial tilting and zonal shift of the NAO pattern is proposed in terms of both the linear Rossby wave theory in slowly varying media and a weakly nonlinear analytical solution. It has been demonstrated that the difference of the spatial tilting of the NAO between its two phases is mainly attributable to the difference of the NAO-induced jet stream between the two phases. In particular, because the difference of the Atlantic jet stream between the positive and negative NAO phases is more (less) distinct in the higher (lower) latitudes, the eastward shift of the northern center of the NAO pattern becomes more prominent. In this case, it is inevitable that the northern center of the NAO pattern exhibits a prominent eastward shift from P1 to P2 when the negative (positive) phase of the NAO is dominant during P1 (P2) (Hurrell 1995). On the other hand, Part I further shows from observational and theoretical aspects that the eastward shift of the Atlantic storm-track eddy activity plays a key role in the eastward shift of the center of action of the NAO pattern during P2 compared to P1. This result is new and different from the previous dynamical explanation of the eastward shift of the center of the NAO pattern during P2 (Peterson et al. 2003; Luo and Gong 2006; Johnson et al. 2008).

However, many questions regarding the dynamics of the NAO pattern are still unsolved in Part I because of the limitations of both the linear Rossby wave theory in slowly varying media and the weakly nonlinear analytical solution. In particular, whether the results found in Part I can be reproduced in numerical models (linear and fully nonlinear numerical models) is an important question that needs to be further addressed. It is also unclear what factors affect the spatial tilting and zonal shift of eddy-driven NAO patterns and what role the Northern Hemisphere (NH) topography plays. The purpose of the present paper is to use linear and fully nonlinear numerical models to investigate factors affecting the spatial tilting and zonal shift of the eddy-driven NAO pattern.

This paper is organized as follows. In section 2, the linear and nonlinear numerical experiments in a sheared basic flow with no forcing are performed to examine how an initial dipole anomaly propagates in a prescribed westerly jet. On this basis, it is easy to identify how the meridional shift of a prescribed jet affects the spatial structure of an evolving Rossby dipole anomaly. In section 3, we introduce a fully nonlinear quasigeostrophic barotropic NAO model with a wavemaker that mimics the Atlantic storm-track eddy activity and with the wavenumber-2 topography used as an approximation of NH topography. Then some numerical results are presented to describe the total fields and time scales of eddy-driven NAO events. In section 4, we identify what factors affect the spatial tilting of eddy-driven NAO patterns. Moreover, the impact of the zonal position of the synoptic-scale wavemaker on the spatial structure and zonal shift of the eddy-driven NAO pattern is examined in section 5. Conclusions and discussion are given in section 6.

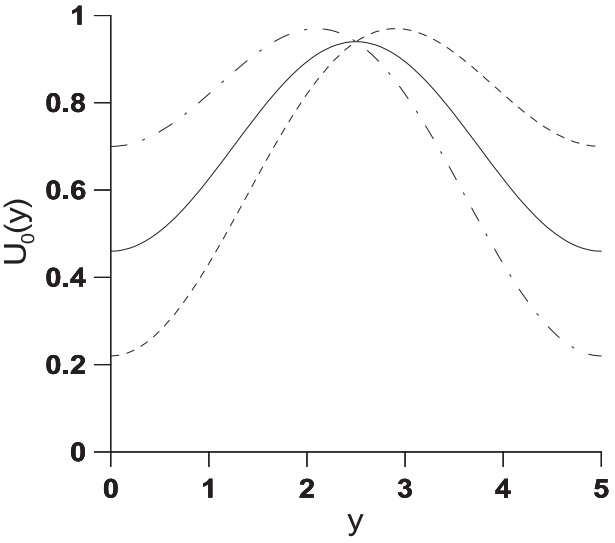

FIG. 1. Meridional distribution of a prescribed jet. The solid curve represents a symmetric jet ($\alpha_2 = 0$), and the dashed and dotted–long dashed lines represent the northward- ($\alpha_2 = -0.24$) and southward-shifting ($\alpha_2 = 0.24$) jets.

2. Propagation of a Rossby dipole anomaly in a prescribed jet in linear and nonlinear models without forcing

a. Linear numerical experiment

In Part I we have used the phase speed formula of the linear Rossby wave in a slowly varying media to investigate how the phase speed of a dipole anomaly depends on the latitudinal distribution of the basic flow. One may question the results because the assumption of slowly varying media is used. In this section, we use

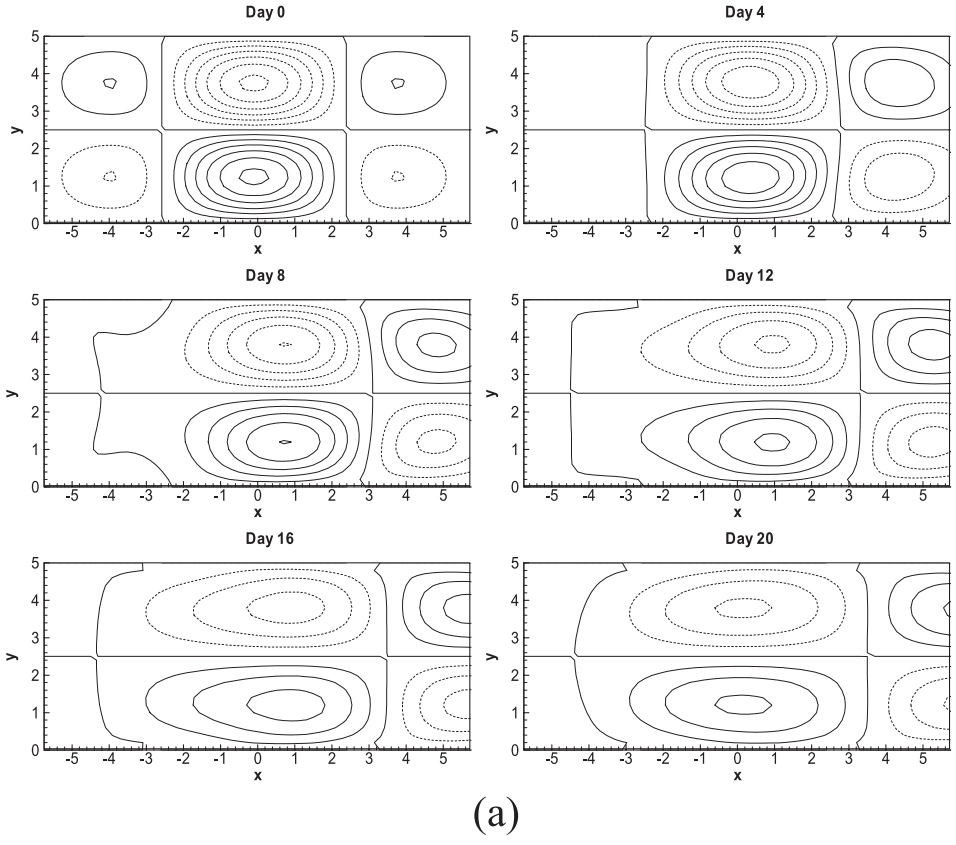

FIG. 2. Evolution of an initial dipole anomaly for the positive phase in a linear model with a prescribed jet: (a) a symmetric jet ($\alpha_2 = 0$), (b) a northward-shifting jet ($\alpha_2 = -0.24$), and (c) a southward-shifting jet ($\alpha_2 = 0.24$). Contour interval is 0.05.

a linear barotropic model to confirm the validity of the linear Rossby wave theory in the slowly varying media used by Part I.

In addition, by performing a series of linear numerical experiments we can understand how a dipole Rossby anomaly propagates in a sheared basic flow $U_0(y)$ and how its spatial structure is affected by the meridional shift of a prescribed jet.

To accomplish our calculations, we restrict our model to a β-plane channel. For a nondivergent atmosphere, the linearized barotropic vorticity (BV) equation in a β-plane channel can be written as

$$\left(\frac{\partial}{\partial t} + U_0\frac{\partial}{\partial x}\right)\nabla^2\psi + (\beta - U_0'')\frac{\partial\psi}{\partial x} = 0, \qquad (1)$$

where ψ is the atmospheric streamfunction anomaly; $U_0(y)$ is the basic flow with a meridional shear; L_y is the width of the β-plane channel; $\nabla^2 = \partial^2/\partial x^2 + \partial^2/\partial y^2$; x and y are the coordinates in zonal and meridional directions, respectively; $\beta = \beta_0 L^2/U_0$ is the meridional gradient of the Coriolis parameter centered at ϕ_0, in which $L = 1000$ km and $U_0 = 10$ m s^{-1} are considered as the characteristic length and velocity of horizontal motions; and $U_0'' = d^2U_0/dy^2$.

The model is required to satisfy a periodic boundary condition in the zonal direction and to satisfy

$$\frac{\partial^2\overline{\psi}(y, t)}{\partial t\partial y} = 0$$

and $\partial\psi/\partial x = 0$ at $y = 0, L_y$ in the meridional direction in which the overbar denotes a zonal average.

Equation (1) is approximated by a standard, second-order, finite difference in a β-plane channel. The spatial derivative is approximated by the central differential scheme, whose space grids in the x and y directions are uniform with $\Delta x = \Delta y = 0.2$. A leapfrog scheme is used for time stepping of the model, and an Euler backward step is used every 50 steps to eliminate time splitting (Holland and Lin 1975). The time step is $\Delta t = 0.072$ for the linear model and $\Delta t = 0.036$ for the nonlinear model. To obtain the streamfunction (ψ) solution, the successive overrelaxation (SOR) method was used to solve the

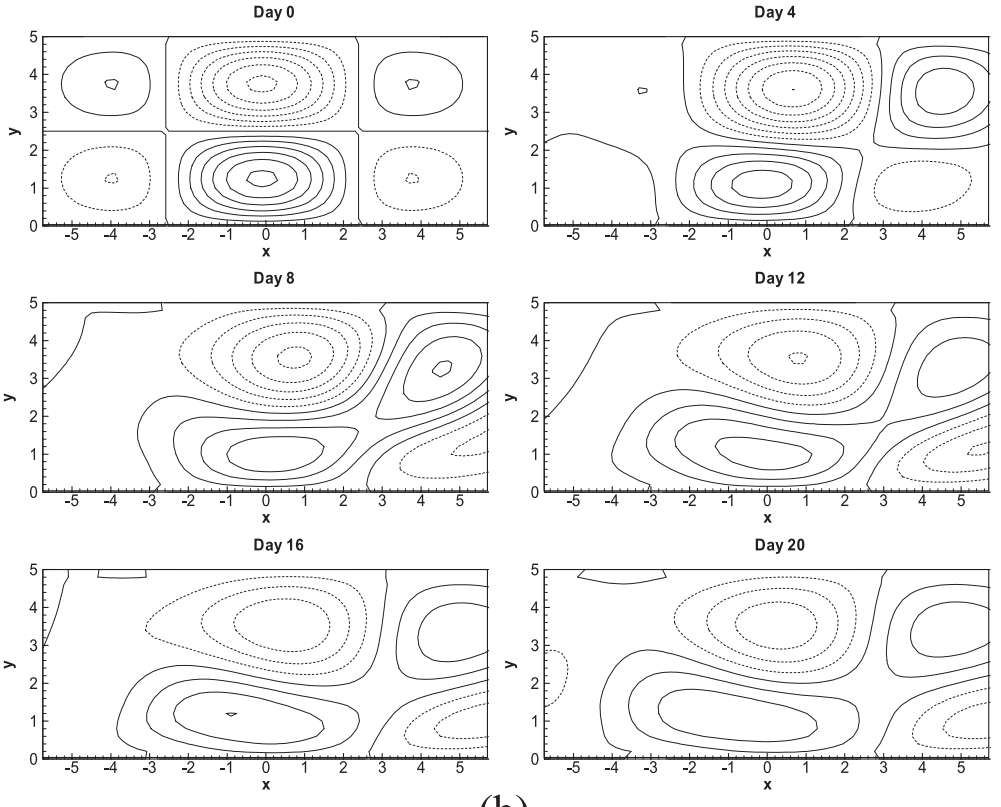

(b)

FIG. 2. (*Continued*)

Poisson equation. In the numerical experiments, a biharmonic dissipation term, which is also used in the nonlinear numerical experiments, is included to insure that all numerical computations are stable.

Using linear Rossby wave theory in the slowly varying media in Part I, we have demonstrated that the phase speed of the dipole anomaly is large (small) in higher latitudes where the core of the westerly jet is in the north (south). This result is at least qualitatively acceptable although the observed Atlantic jet distribution (Part I, Fig. 4) does not strictly satisfy the assumption of slowly varying media. To examine whether the result predicted by using the linear Rossby wave theory in a slowly varying media is correct, here we consider a highly idealized jet even though it does not satisfy the assumption of the slowly varying media.

As in Luo et al. (2008), the prescribed westerly jet can be assumed to be

$$U(y) = u_0 - \alpha_1 \cos(my) + \alpha_2 \cos(my/2), \qquad (2)$$

where u_0 is the strength of uniform basic westerly wind, α_1 is the strength of a symmetric jet, and α_2 is the strength of the prescribed jet shifting from a symmetric jet.

Here we fix $u_0 = 0.7$ and $\alpha_1 = 0.24$ but allow α_2 to vary in order to allow the different latitudinal position of the jet core. Figure 1 shows the meridional distribution of a jet for three cases: $\alpha_2 = 0$, $\alpha_2 = 0.24$, and $\alpha_2 = -0.24$. It is easily seen in this figure that $\alpha_2 = -0.24$ ($\alpha_2 = 0.24$) represents that the core of the jet is in higher (lower) latitudes, while $\alpha_2 = 0$ corresponds to a symmetric jet. Thus, $\alpha_2 = -0.24$ ($\alpha_2 = 0.24$) corresponds to a jet shifting to the north (south). In subsequent discussions, the asymmetric jet is referred to as ''shifting jet.'' To examine whether the latitudinal position of the jet core affects significantly the zonal propagation of a dipole anomaly in the different latitudes, without the loss of generality, we assume that the initial dipole anomaly is of the form

$$\psi|_{t=0} = B_0 \sqrt{\frac{2}{L_y}} \exp(ikx) \exp(-\gamma x^2) \sin(my) + \text{c.c.} \qquad (3)$$

in which $k = 2k_0$ $\{k_0 = 1/[6.371 \cos(\phi_0)]\}$ is the zonal wavenumber of the initial dipole anomaly with both amplitude B_0 and zonal wavenumber 2, $\gamma > 0$ denotes the zonal localization of the corresponding initial value,

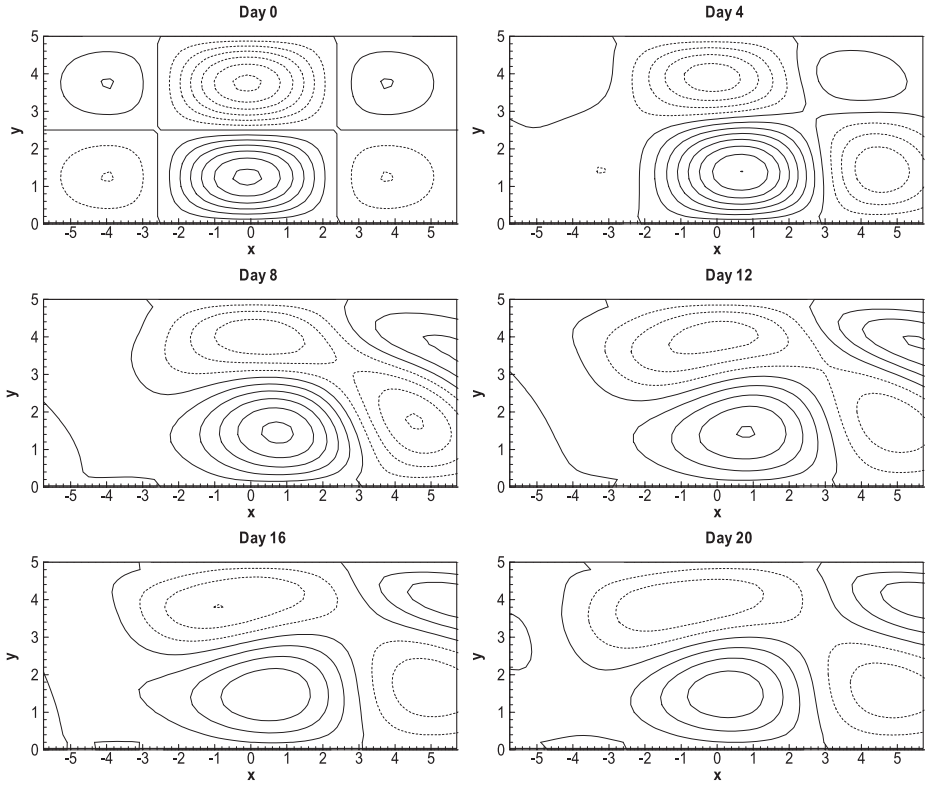

(c)

FIG. 2. (*Continued*)

and c.c. represents the complex conjugate of its preceding term.

In this paper, we choose $\varphi_0 = 55°\text{N}$, $u_0 = 0.7$, $\gamma = 0.5$, and $B_0 = 0.4$ as fixed parameters in the linear and nonlinear numerical experiments with no forcing. It is also noted that $m > 0$ ($m < 0$) denotes the positive (negative) phase. In the experiments, it is useful to define $\psi_A = \sum_{n=1}^{4} \psi_n(x, y, t)$ as the planetary-scale streamfunction anomaly of the evolving Rossby dipole mode in a sheared basic flow in which ψ_n (n = 1, . . . , 4) denotes the wave components with zonal wavenumbers 1–4 of the total streamfunction field $-\int_0^y U(y')dy' + \psi$. For a comparison, $\psi_A = \sum_{n=1}^{4} \psi_n(x, y, t)$ is still used as a planetary-scale anomaly of eddy-driven NAO events in subsequent nonlinear numerical experiments with forcing.

Figure 2 shows the evolution of an initial dipole mode in a prescribed jet for the positive phase ($m > 0$). It is found that in a symmetric jet the initial dipole mode propagates slowly eastward, and the dipole anomaly pattern is almost always symmetric in the meridional direction (Fig. 2a). This situation can be altered once the westerly jet becomes an asymmetric jet. The initial dipole mode can evolve into a NE–SW tilted dipole as the jet core is in the higher latitudes (Fig. 2b) but a NW–SE tilted dipole if the jet core is in the lower latitudes (Fig. 2c). It is easily verified that the above result is also tenable for the negative phase ($m < 0$) because Eq. (1) is invariant with respect to parity (not shown). This is clearly seen by making the transformation $\psi \rightarrow -\psi$. That is to say, when the core of the westerly jet is in the higher (lower) latitudes, the negative phase dipole anomaly can exhibit a NE–SW (NW–SE) tilting. Thus, the tilting direction of the Rossby dipole mode in a prescribed jet is determined by the latitudinal position of the jet core, rather than by the phase of the dipole mode. When the jet core undergoes a northward (southward) shift, the subsequent dipole mode exhibits a NE–SW (NW–SE) tilting regardless of its phase. These results are in agreement with the prediction of the linear Rossby wave propagation in slowly varying media in Part I even though the assumption of slowly varying media is not strictly satisfied. It is noteworthy that all dipole anomalies decay in time towing to the inclusion of a dissipation term in the numerical calculation of Eq. (1). Even so, the linear numerical experiments performed here indicate that the propagation theory of the linear Rossby wave in a slowly varying media can be used to predict how the spatial structure of the dipole

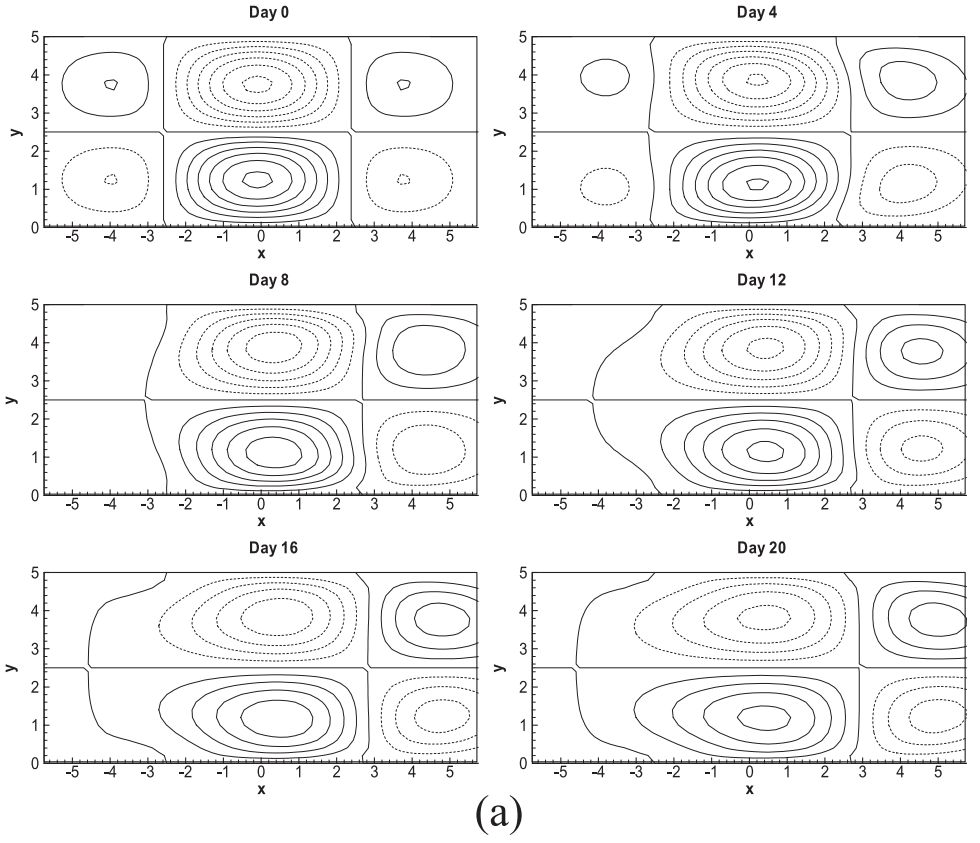

FIG. 3. As in Fig. 2 but in a nonlinear model.

anomaly depends on the latitudinal distribution of a prescribed jet.

b. *Nonlinear numerical experiments without any forcing*

An important question that we should address here is whether the above conclusion is also true in a nonlinear framework without any forcing (topography and storm-track eddy forcing and so on). Here we will perform a nonlinear numerical experiment to examine this question. If the term of $J(\psi, \nabla^2\psi)$ is added in the left-hand side of Eq. (1), it becomes a nonlinear BV equation in a sheared basic flow. The numerical method here is the same as that used in solving Eq. (1), but the Jacobian term $J(\psi, \nabla^2\psi)$ is evaluated using the Arakawa scheme, which conserves kinetic energy and enstrophy and maintains the property $J(A, B) = -J(B, A)$ (Arakawa 1966).

A series of nonlinear numerical experiments are performed in this subsection. Here we only present the result of the positive phase. Figure 3 shows the result of the nonlinear BV model for the same model parameters as in Fig. 2. It is found that in a nonlinear model with no forcing the evolution of a dipole anomaly in a sheared basic flow exhibits the same characteristics as that in a linear model (Fig. 2), although the spatial tilting of the dipole anomaly is less prominent in a nonlinear model than in a linear model. This result is also tenable for the negative phase (not shown). This indicates that the results predicted by the linear Rossby wave propagation theory in a slowly varying media hold in both linear and nonlinear models without forcing.

3. The fully nonlinear quasigeostrophic barotropic NAO model

a. *Fully nonlinear quasigeostrophic barotropic model*

In section 2, we have examined how the latitudinal distribution of the basic flow affects the spatial shape and propagation of an initial dipole anomaly in the zonal direction by solving linear and nonlinear unforced models. These experiments confirm the validity of the linear Rossby wave propagation theory in the slowly varying media used in Part I and further demonstrate that the result predicted by the linear theory is also correct in a nonlinear BV model without forcing. However, when the eddy-driven NAO anomaly grows to a large amplitude stage, whether the above result still holds is unclear. This problem will be investigated in this section. Additionally, to reveal what

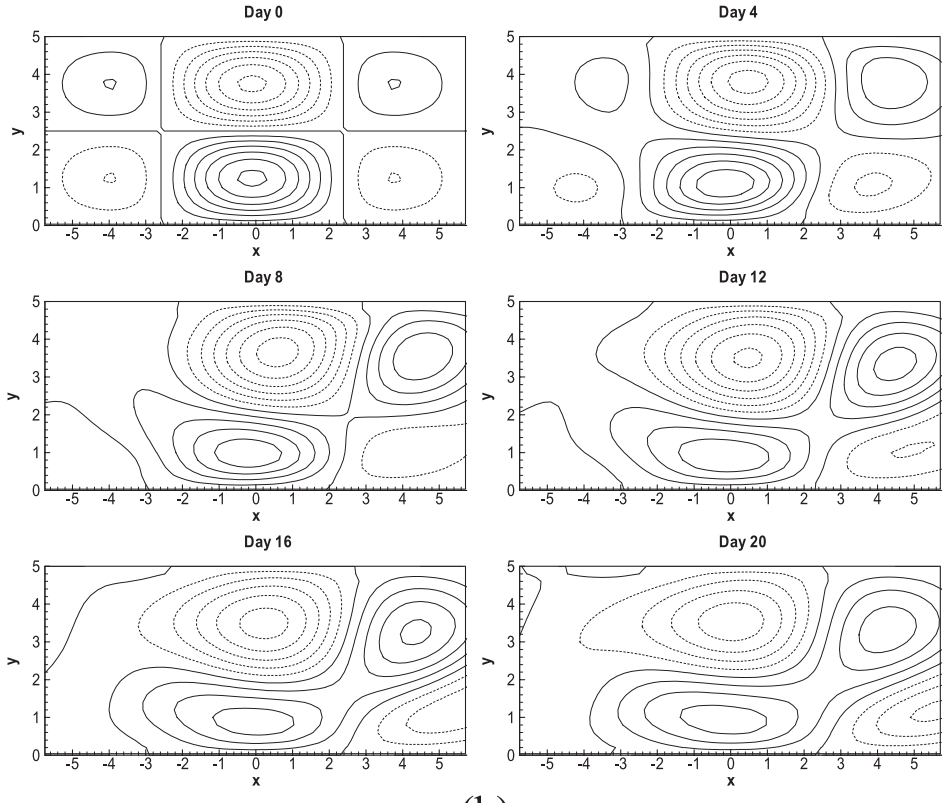

(b)

FIG. 3. (*Continued*)

factors affect the spatial tilting and zonal shift of the eddy-driven NAO pattern, it is necessary to numerically solve a fully nonlinear quasigeostrophic BV equation with large-scale topography (two oceans and continents) in the NH and with the synoptic-scale wave forcing.

Similar to Luo (2005), the nondimensional nonlinear quasigeostrophic BV equation used here is assumed to be of the form

$$\frac{\partial}{\partial t}(\nabla^2\Psi - F\Psi) + J(\Psi, \nabla^2\Psi + h) + \beta\frac{\partial\Psi}{\partial x} = F_s, \quad (4)$$

where Ψ is the total streamfunction of atmospheric motions, h is the nondimensional topographic variable, $F = (L/R_d)^2$ in which L is the characteristic length and R_d is the radius of Rossby deformation, F_s is a wave-maker designed to excite synoptic-scale eddies in the Atlantic storm track (Shutts 1983, and the other notation is as in Eq. (1). The zonal boundary condition used here is the same as that in Eq. (1), but the lateral boundary condition is replaced with

$$\frac{\partial^2\overline{\Psi}(y, t)}{\partial t\partial y} = 0$$

and $\partial\Psi/\partial x = 0$ at $y = 0, L_y$.

As in Part I, the total streamfunction of a NAO event in an analytical model can be expressed as $\Psi = \overline{\psi}(y) + \psi_M + \psi_{\mathrm{NAO}} + \psi_C + \psi'$, where $\overline{\psi}(y)$ is the zonal mean flow, ψ_M is the jet stream anomaly that depends on the envelope amplitude of the NAO anomaly, ψ_{NAO} is the NAO anomaly, ψ_C is the stationary wave anomaly induced by the topography, and ψ' is the synoptic-scale waves. For a specified mean flow $\overline{\psi}(y)$, if the large amplitude NAO anomaly ψ_{NAO} can be excited by synoptic-scale waves ψ', the interaction between the NAO anomaly ψ_{NAO} and the stationary wave anomaly ψ_C is able to induce a change in the jet stream anomaly ψ_M. In this case, the zonal mean flow

$$U = U_0(y) - \frac{\partial\psi_M}{\partial y}$$

and

$$U_0(y) = -\frac{\partial\overline{\psi}}{\partial y}$$

in the Atlantic can become time dependent (Luo et al. 2007b). Since the spatial structure of the NAO pattern is dominated by the latitudinal distribution of the zonal

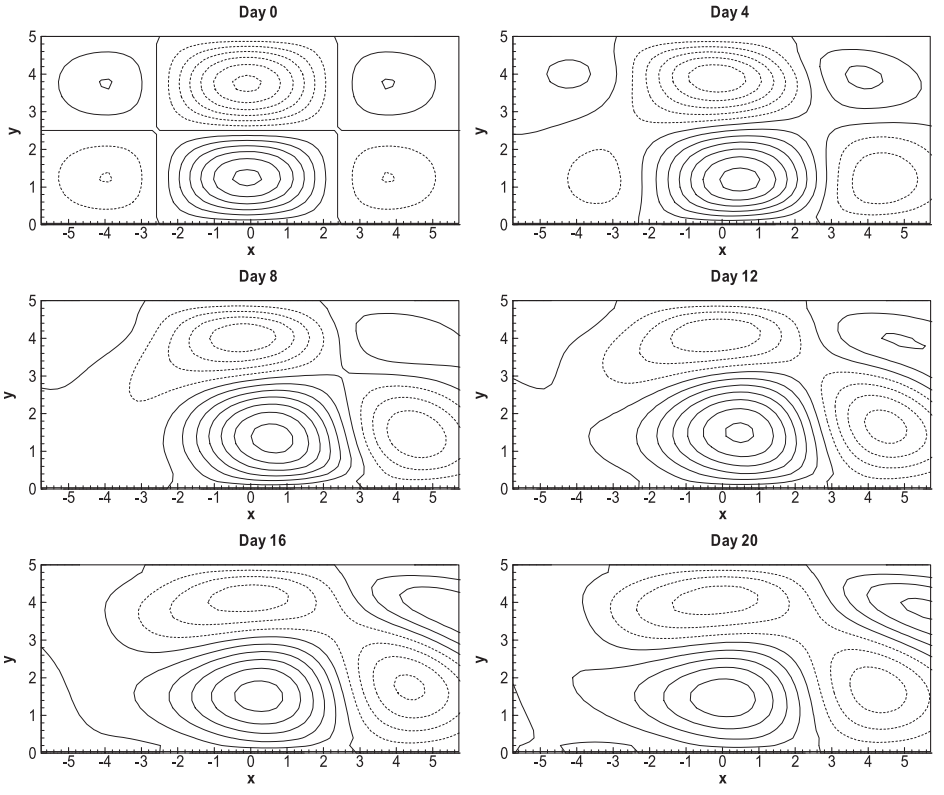

(c)

FIG. 3. (*Continued*)

mean flow U, as described in Part I, it is also reasonable to look at the relationship between the zonal mean flow $U(y, t)$ in the Atlantic and the NAO pattern in our numerical model. Of course, the latitudinal distribution of the prespecified mean flow $\overline{\psi}(y)$ can affect the subsequent NAO event and the variability of the subsequent jet stream anomaly. This can be better understood in terms of the results of the numerical model here once $\overline{\psi}(y)$ is prescribed.

Here the initial synoptic-scale eddies are not prescribed; instead, they are excited by the prespecified synoptic-scale wavemaker F_s, as done in Shutts (1983). The numerical method used here is the same as that used in section 2. The initial dipole planetary wave, regarded as an initial NAO pattern, the wavemaker F_s, and topographic variable h, are assumed to be

$$\Psi|_{t=0} = \psi|_{t=0} + \psi'|_{t=0}, \tag{5a}$$

$$\psi|_{t=0} = -\int_0^y U_0(y')\,dy' + B_0\sqrt{\frac{2}{L_y}}\exp(ikx)\exp(-\gamma x^2)\sin(my) + \text{c.c.}, \tag{5b}$$

$$\psi'|_{t=0} = 0, \tag{5c}$$

$$F_s = 2b_0[\cos(\tilde{k}_1 x - \tilde{\omega}_1 t) + \alpha\cos(\tilde{k}_2 x - \tilde{\omega}_2 t)] \times \sin(m_s y)\exp[-c_0(x + x_s)^2], \tag{5d}$$

and

$$h = h_0\exp(ikx)\sin(m_s y) + \text{c.c.}, \tag{5e}$$

where $m_s = m/2$, $c_0 > 0$, and x_s is the longitudinal position of the prescribed wavemaker with the amplitude of b_0 relative to the initial NAO center at $x = 0$. The value of x_s (c_0) can represent the region (zonal widening) of the eddy activity. When x_s is smaller, the eddy activity excited by the wavemaker shifts to the east, while the small value of c_0 can represent the widening of the eddy activity. Thus, the downstream extension of the Atlantic eddy activity can correspond to decreasing both x_s and c_0. Here $U_0(y)$ is assumed to be the same as in Eq. (2). Moreover,

$$\tilde{\omega}_i = u_0\tilde{k}_i - \frac{(\beta + Fu_0)\tilde{k}_i}{\tilde{k}_i^2 + m_s^2 + F}$$

($i = 1, 2$) is the frequency of the synoptic-scale wavemaker comprised of two waves with zonal wavenumbers 9 and 11 ($\tilde{k}_1 = 9k_0$ and $\tilde{k}_1 = 11k_0$). It should be pointed out that there must be $m_s < 0$ and $\alpha = -1$ in Eq. (5d) for the negative phase of NAO events, but $m_s > 0$ and $\alpha = 1$ for the positive phase of NAO events, as indicated in Luo et al. (2007a,b). Here, $h_0 < 0$ ($h_0 > 0$) must be required to represent the Atlantic basin for $m_s > 0$ ($m_s < 0$).

We define $D_s = x_s - x_c$ as the distance of the synoptic-scale wavemaker relative to the center of the initial NAO at $x_c = 0$. In subsequent numerical experiments, the parameters $B_0 = 0.4$, $\gamma = 0.5$, $b_0 = 0.65$, $c_0 = 0.5$, and $u_0 = 0.7$ are fixed, but we allow the varying of x_s.

For $x_s = 2.0$ and $h_0 = 0.2$ (a topographic height of 400 m), we plot the horizontal distribution $h(x, y)$ of the wavenumber-2 topography, as given in Charney and DeVore (1979), the initial dipole anomaly for the negative NAO phase, and the wavemaker F_s in Fig. 4.

In Fig. 4a, the region of dashed curves denotes the Atlantic basin. In our nonlinear numerical experiment, the initial dipole anomaly is assumed to be located at $x = 0$ (the center of the Atlantic basin, Fig. 4b), but the synoptic-scale wavemaker is assumed to locate at $x = -2$ (2000 km) upstream of the initial dipole anomaly (Fig. 4c). By numerically solving Eq. (4), we can examine how synoptic-scale eddies produced by this wavemaker excite a NAO event for a given initial value.

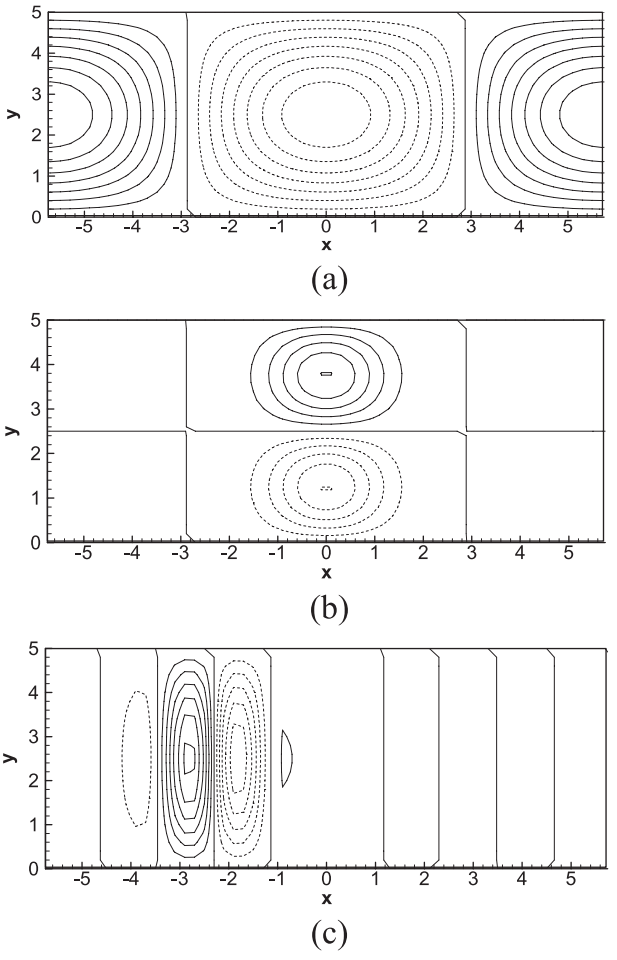

FIG. 4. (a) Horizontal distributions of the topography $h(x, y)$, (b) the initial dipole anomaly for the negative NAO phase, and (c) the wavemaker F_s for $b_0 = 0.65$ and $c_0 = 0.5$. The contour interval is 0.05 in (a) and 0.2 in (b) and (c).

b. Eddy-driven NAO events

In the absence of topography, Fig. 5 shows the instantaneous total streamfunction fields Ψ of eddy-driven NAO events for the negative ($\alpha = -1$ and $m = -2\pi/L_y$) and positive ($\alpha = 1$ and $m = 2\pi/L_y$) phases in a prior uniform basic flow with $\alpha_1 = 0$ and $\alpha_2 = 0$. Here, day 0 is defined to be the time after one day of integration of Eq. (1) because the beginning of Eq. (1) does not contain synoptic-scale waves. It is found in Fig. 5 that the spatial pattern and life duration of eddy-driven NAO events bear a striking resemblance to observed NAO events (Luo et al. 2007a, their Fig. 6), which are also basically consistent with the weakly nonlinear analytical solutions derived by Luo et al. (2007a). In fact, Fig. 5a looks like a classical blocking flow. Luo et al. (2007a) and Woollings et al. (2008), however, noted that the negative-phase NAO event is in essence identical to a blocking flow. Thus, it is reasonable to say that Fig. 5a is similar to the observed negative-phase NAO event. Also a similar result exists in the presence of topography (not shown). At the same time, for the negative (positive) phase, cyclonic (anticyclonic) wave breaking can be visible in the total fields. Thus, it is concluded that the cyclonic (anticyclonic) wave breaking is a main cause of the occurrence of the negative (positive) phase of the NAO event (Benedict et al. 2004; Franzke et al. 2004; Woollings et al. 2008).

Of course, the detailed structure of the total field of the NAO event is also found to depend on the strength of the synoptic-scale wavemaker and its zonal localization or width. For example, Fig. 6 shows the total fields of the NAO events for $b_0 = 0.8$ and $c_0 = 0.25$. It is noted that, when the synoptic-scale wavemaker is stronger and is concentrated in a wider zonal region, the small-scale cyclonic and anticyclonic vortices within the NAO region become more intense so that the total fields of the model NAO events for the positive and negative phases are probably more similar to observed

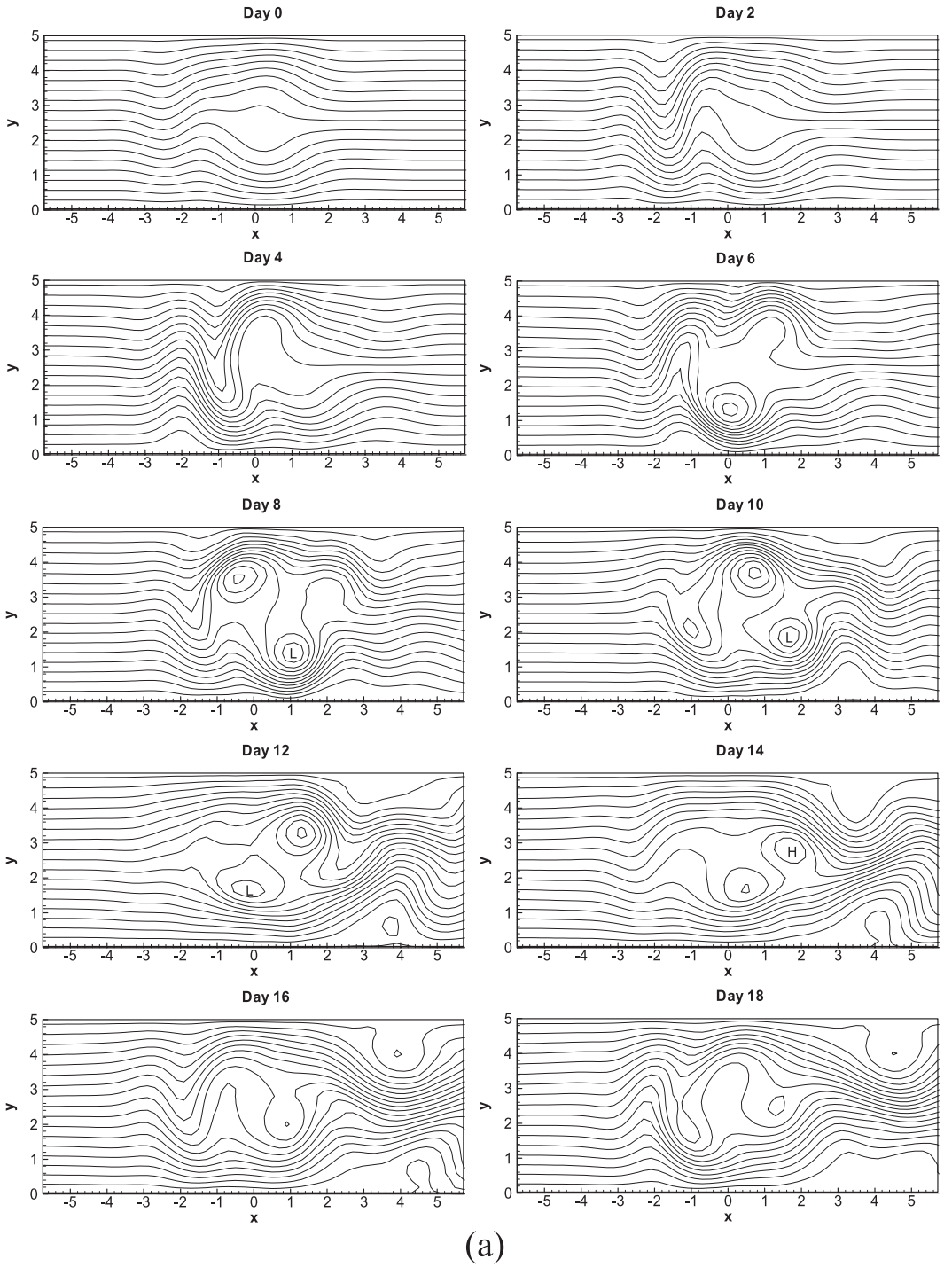

FIG. 5. Instantaneous total fields of eddy-driven NAO events in a nonlinear model simulation for a wavemaker for $b_0 = 0.65$ and $c_0 = 0.5$ in a prior uniform basic flow and in the absence of topography: (a) negative and (b) positive phases. Contour interval is 0.2.

NAO events (Benedict et al. 2004; Luo et al. 2007a). This result also holds even for higher topography, but the NAO pattern has a different detailed structure (not shown).

c. Time scales of model NAO events

Before this model is used to investigate the physical dynamics of NAO events, we first examine if the life

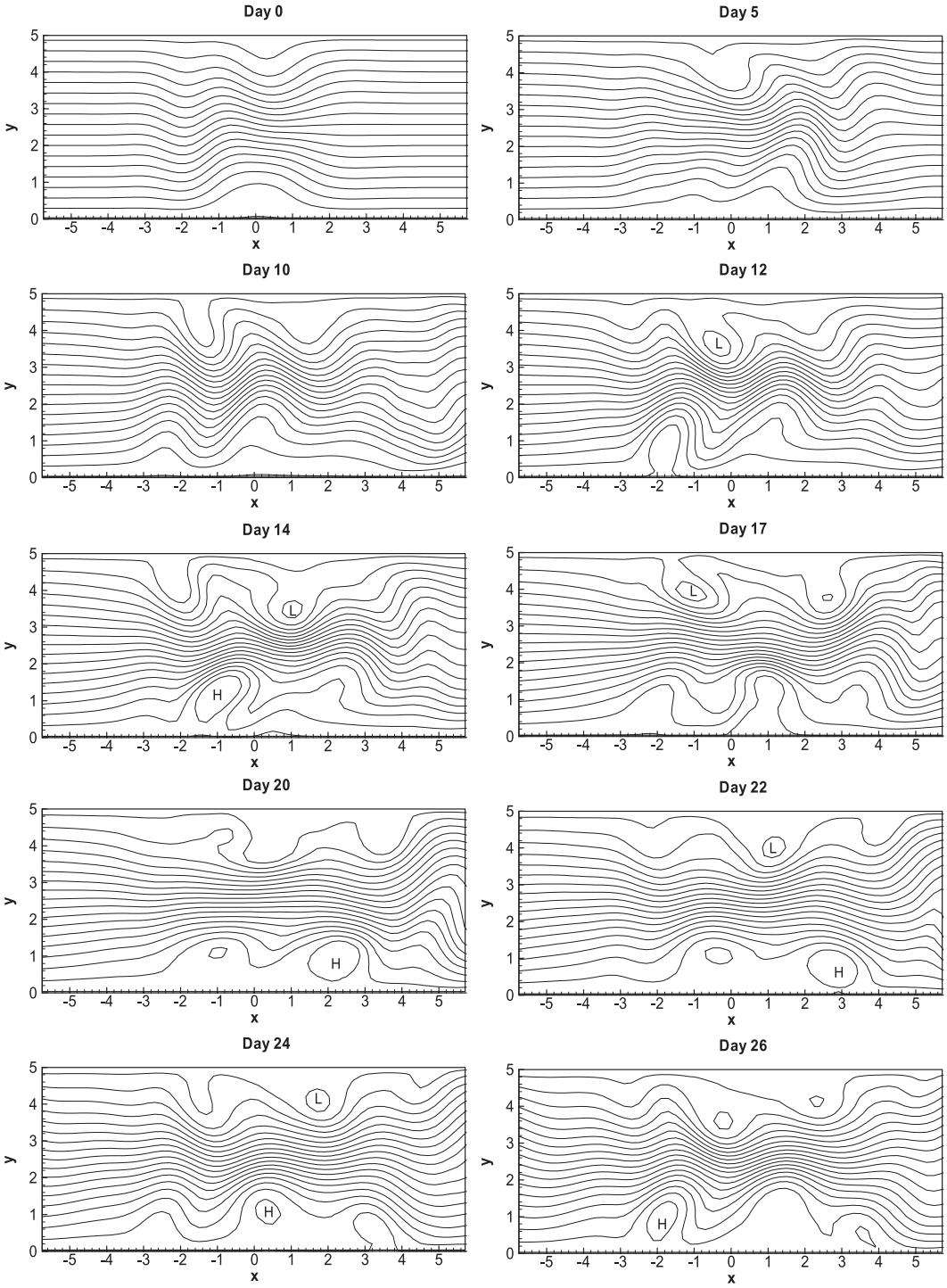

(b)

FIG. 5. (*Continued*)

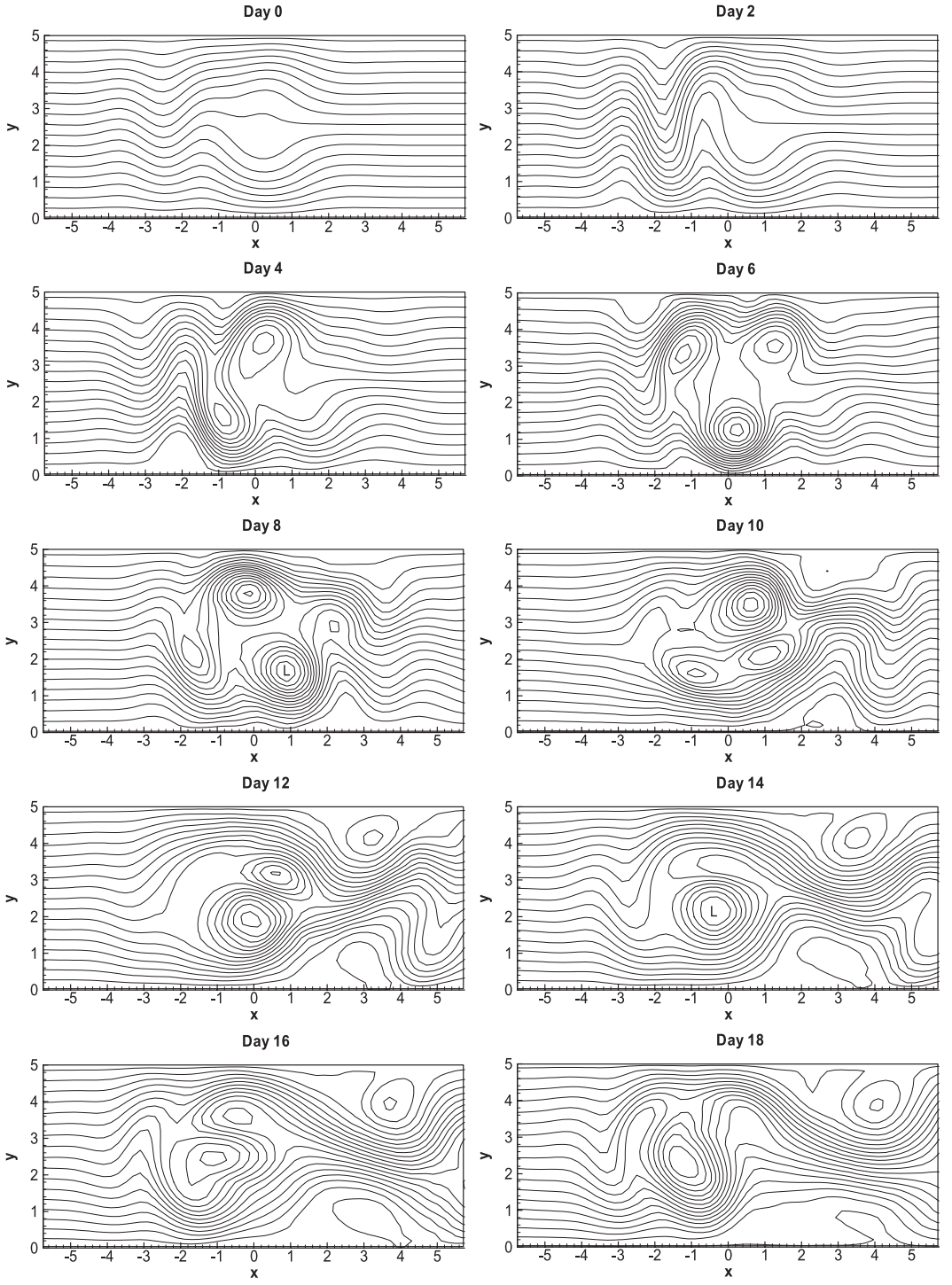

FIG. 6. As in Fig. 5 but for $b_0 = 0.8$ and $c_0 = 0.25$.

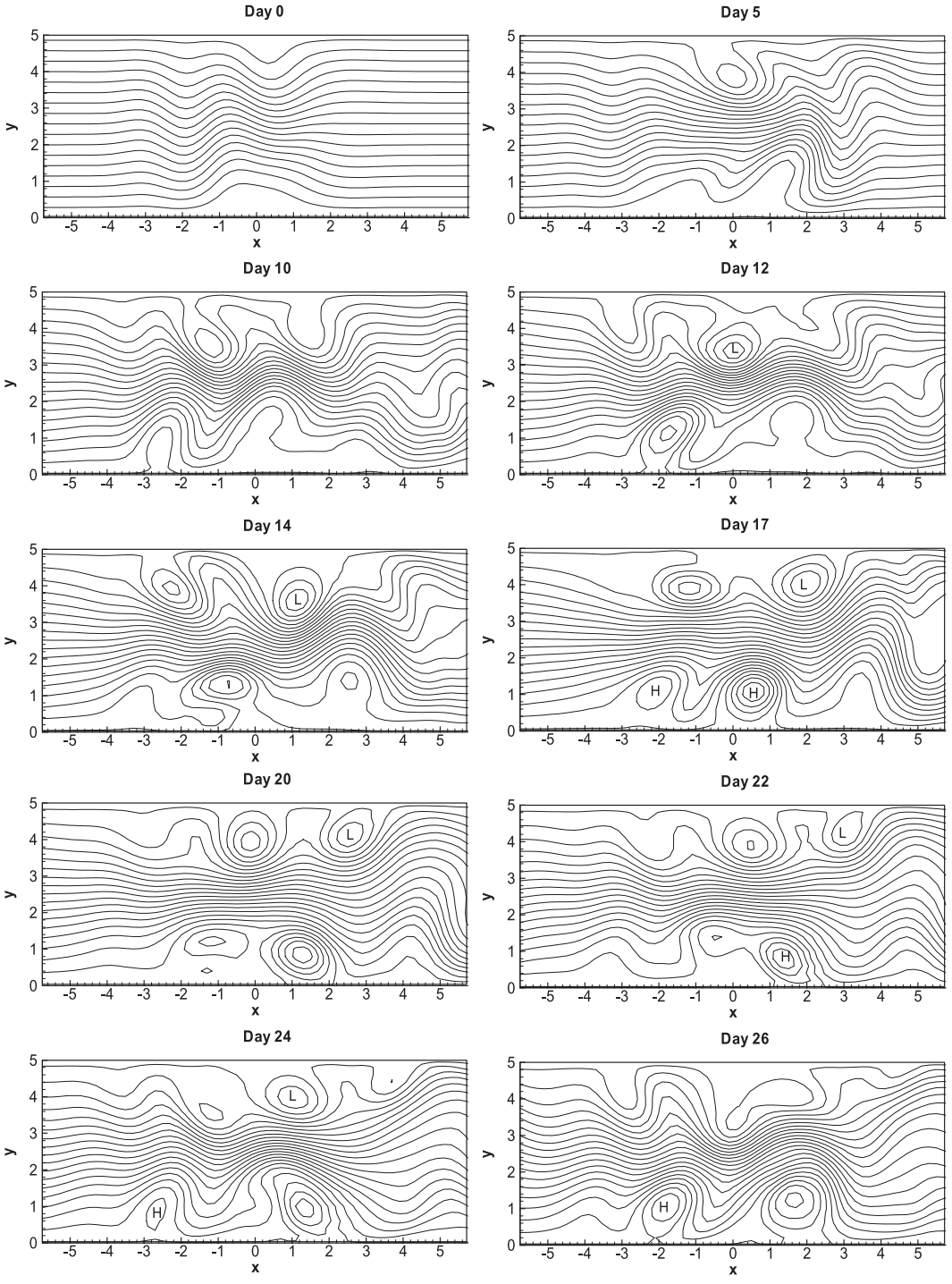

(b)

FIG. 6. (*Continued*)

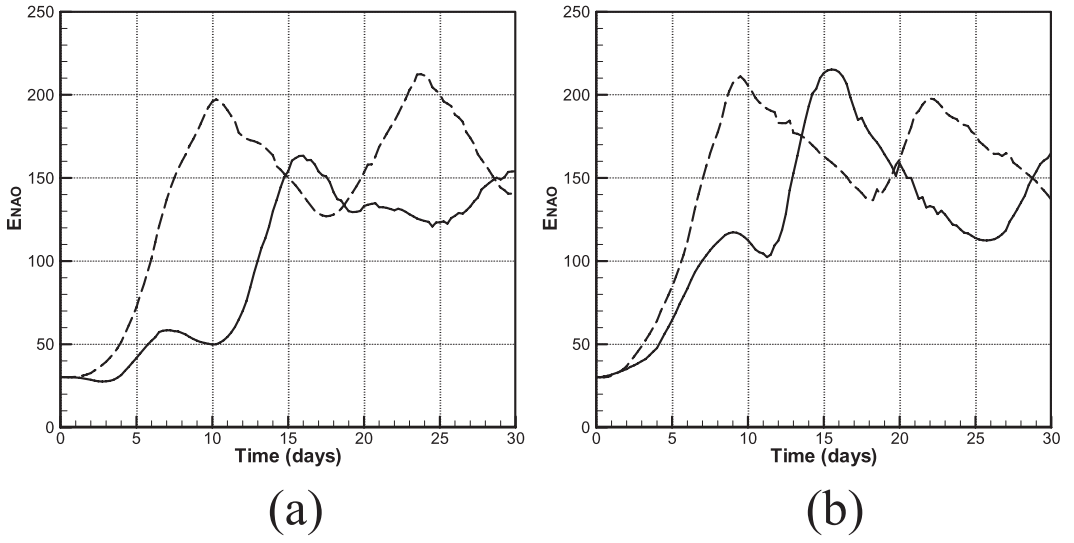

FIG. 7. Time evolution of the total kinetic energy of the eddy-driven NAO anomaly in a prespecified uniform background flow for two cases: (a) without topography and (b) with topography. The solid (dashed) line denotes the positive (negative) NAO phase.

periods of NAO events reproduced in the nonlinear barotropic model used here are consistent with the durations of observed NAO events. Under different conditions we calculate the total kinetic energy (TKE) of the NAO anomaly by defining

$$E_{\mathrm{NAO}} = \frac{1}{2}\iint_{\sigma} (u_P^2 + v_P^2)\, dx\, dy,$$

where $(u_P, v_P) = (-\partial\psi_A/\partial y, \partial\psi_A/\partial x)$ is defined for $\psi_A = \sum_{n=1}^{4}\Psi_n$ (Ψ_n is each one of zonal wavenumber 1–4 components of Ψ) and σ denotes the horizontal area of the NAO anomaly. In the absence and in the presence of topography, Fig. 7 shows the time evolution of the total kinetic energy E_{NAO} of the eddy-driven NAO anomaly in a prior uniform westerly wind for two cases without and with topography. It is found that for the period of 30 days the TKE for the negative phase can have two life cycles (the second cycle can reoccur after the first event decays), but one life cycle is dominant for the positive phase. For each cycle of the negative phase NAO, the time scale of the TKE in growth and decay is

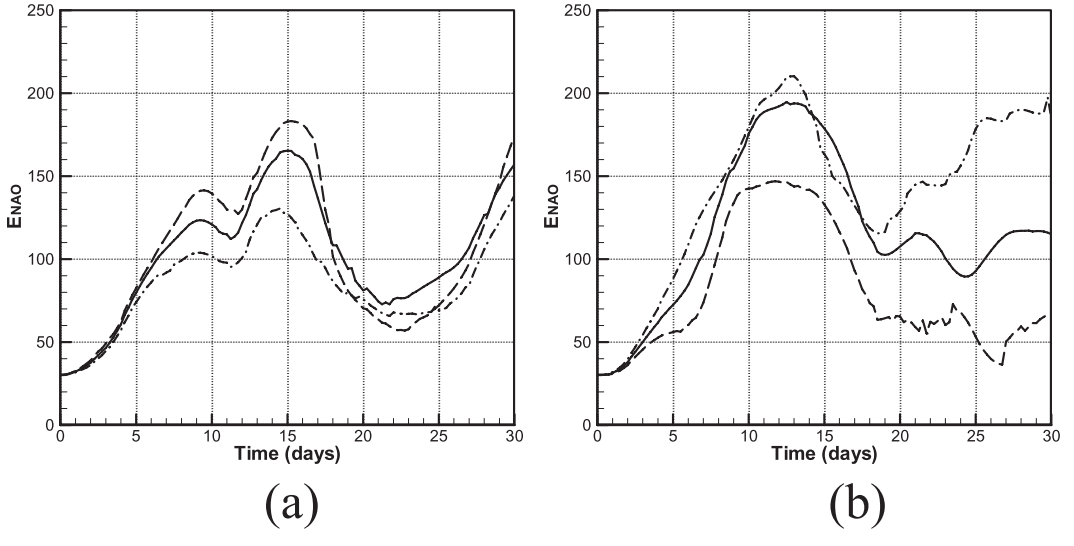

FIG. 8. Time evolution of the TKE of the eddy-driven NAO anomaly in the presence of topography and prespecified shifting jet for the (a) positive and (b) negative NAO phases. The solid line represents a symmetric jet; the dashed (dotted–dashed) line denotes the southward (northward)-shifting jet.

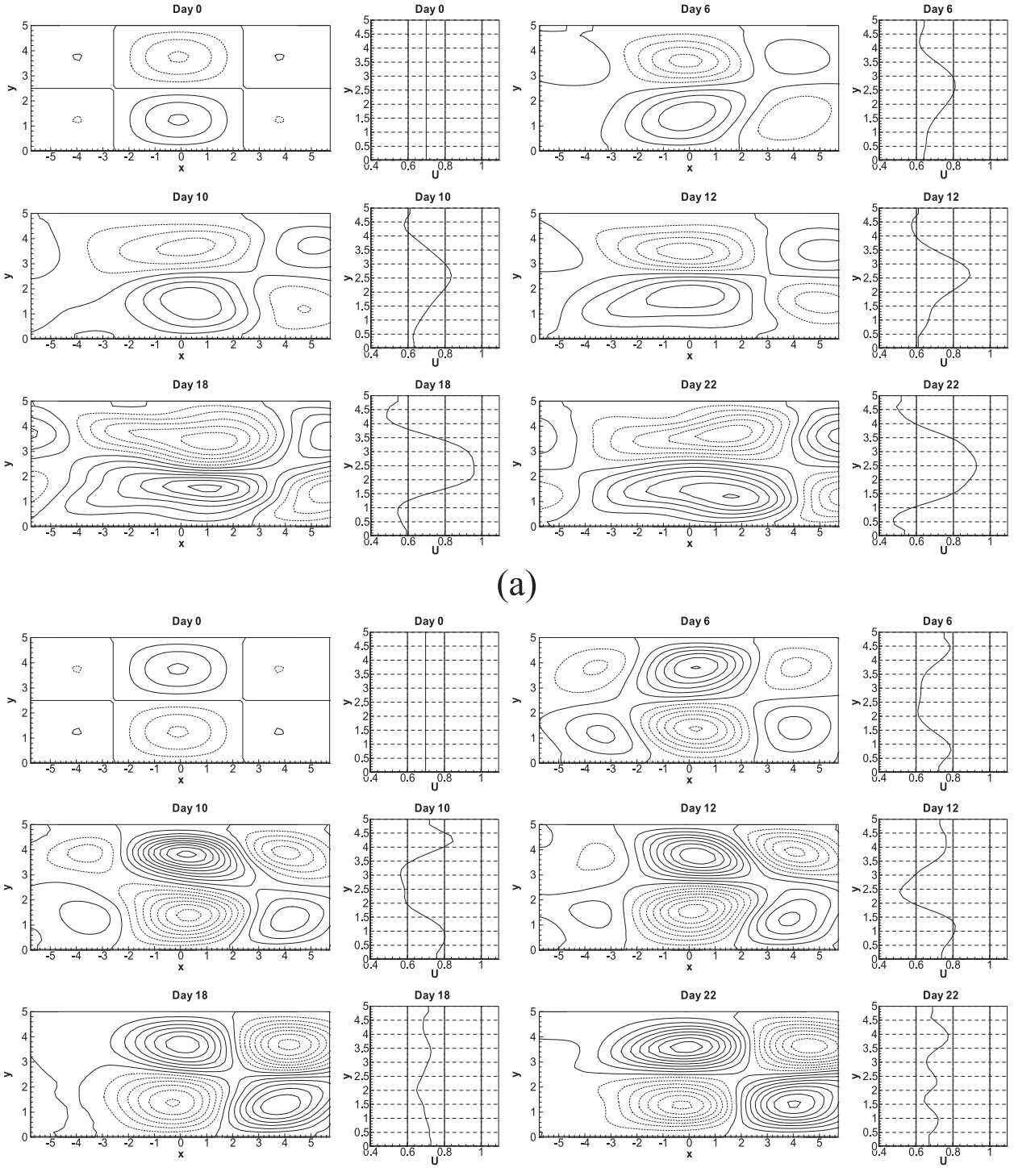

FIG. 9. Instantaneous time sequences of the streamfunction anomaly ψ_A and time-dependent mean flow $U(y, t)$ of the eddy-driven NAO pattern in the absence of topography and for a prespecified uniform basic flow: (a) positive and (b) negative NAO phases. Contour interval is 0.1.

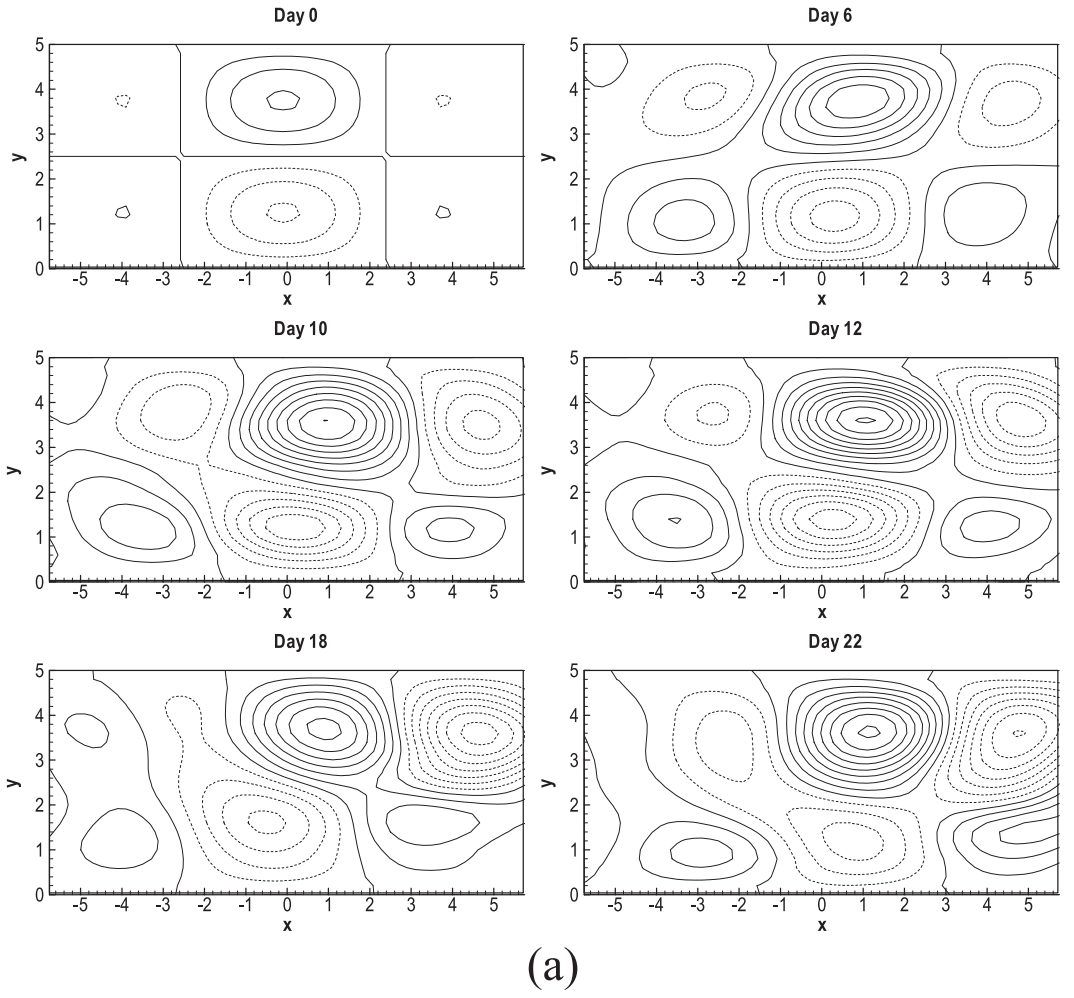

FIG. 10. Streamfunction anomaly ψ_A of the eddy-driven negative NAO phase pattern in the absence of topography for the prespecified (a) northward- and (b) southward-shifting jets. Contour interval is 0.1.

approximately 10–20 days (two weeks). Although the TKE of the positive phase NAO exhibits one peak, its dominant growth and decay period is ~10–20 days. Thus, the eddy-driven NAO event can have a lifetime of ~10–20 days (two weeks) for its two phases. This is basically in agreement with the observational finding by Feldstein (2003) and the theoretical result by Luo et al. (2007a), who indicated that the intrinsic time scales of NAO events are of about two weeks (10–20 days). This also holds even in the presence of topography. In addition, it is noted that the TKE of the eddy-driven NAO anomaly is enhanced in the presence of topography. Figure 8 shows the case with both topography and a prespecified shifting jet. It is found that although the meridional position of the prescribed shifting jet can affect the TKE of the eddy-driven NAO anomaly in growth and decay, the strong growth and decay of the NAO still occur on the 10–20-day (two week) time scale. Thus, the numerical solutions performed here can capture the intrinsic time scales of observed NAO events. Because of the efficiency of this numerical model in capturing the main characteristics of the NAO, the model can be used to investigate what factors affect the spatial tilting and zonal shift of eddy-driven NAO anomalies.

4. Spatial structures of eddy-driven NAO patterns in a fully nonlinear barotropic model

Although the basic flow before the NAO event begins is assumed to be time independent in our experiments, the subsequent basic flow accompanying the occurrence of NAO events will become time dependent due to the feedback of the NAO anomaly and its interaction with a topographic wave. For this case, the jet stream and NAO anomalies are coupled together. However, to

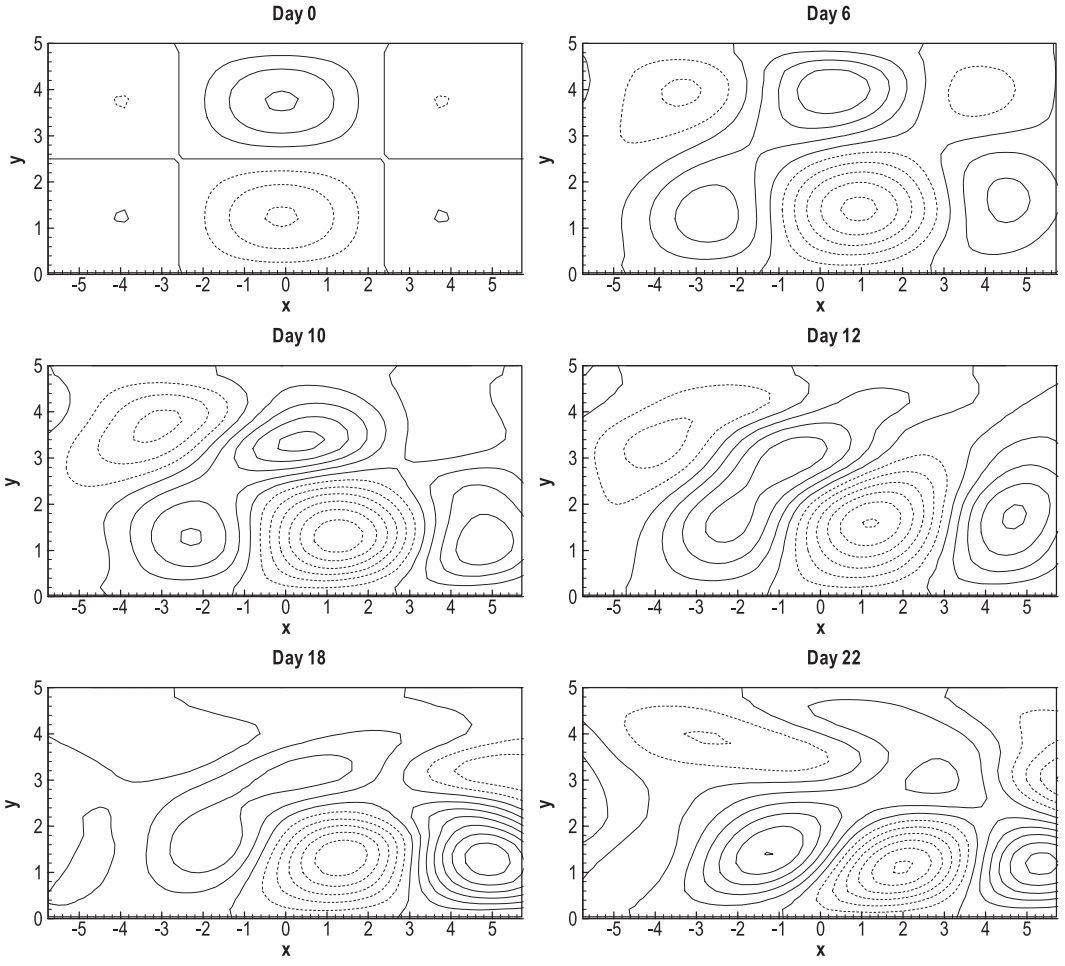

(b)

FIG. 10. (*Continued*)

clearly see how the basic flow depends on the different stages of the NAO, the zonal wavenumber-0 component of the zonal westerly wind during the NAO life cycle can be considered as the time-dependent zonal mean flow $U(y, t)$.

a. *Spatial structures of eddy-driven NAO patterns in a prespecified uniform background flow, but with no topography*

In this experiment, we first consider a uniform background flow $U_0(y) = u_0$ [u_0 is a constant as in Eq. (2)] at an initial stage and assume that the large-scale topography is absent ($h = 0$) in order to allow a comparison of the results with a shifting jet or with the topography. For the same model parameters as in Fig. 5, the instantaneous time sequences of the streamfunction anomaly ψ_A of the eddy-driven NAO pattern and time-dependent zonal mean flow $U(y, t)$ are shown in Fig. 9 for its two phases.

An initial dipole can evolve into a NAO dipole anomaly under the forcing of transient synoptic-scale waves. For its positive and negative phases the eddy-driven NAO pattern is almost symmetric in the meridional direction when the basic flow prior to the NAO onset is uniform. This is basically consistent with the result of the weakly nonlinear NAO model proposed by Luo et al. (2007a). Moreover, during the NAO life cycle a single jet (two weak jets) can be formed for the positive (negative) NAO phase, but the meridional shift of the jet core seems less distinct. This indicates that the north–south shift of the jet core accompanying the occurrence of subsequent NAO events is relatively weak in the absence of topography if the prespecified basic flow is uniform. Nevertheless, it should be noted that this result is based on a Cartesian model (β plane) and the result

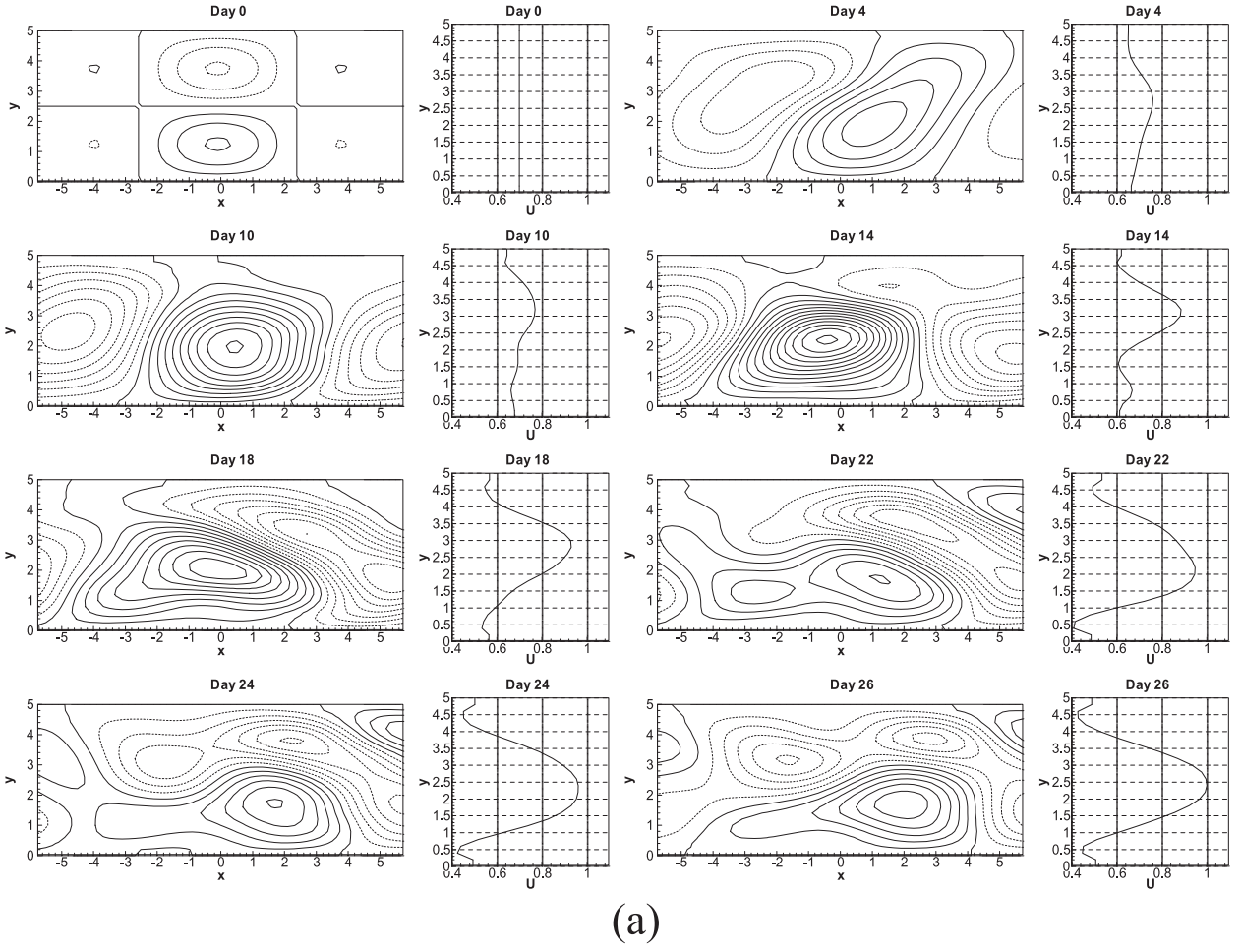

FIG. 11. Instantaneous time sequences of the streamfunction anomaly ψ_A and the time-dependent mean flow $U(y, t)$ of the eddy-driven NAO pattern for a uniform westerly wind prior to NAO onset in the presence of topography: (a) positive and (b) negative NAO phases. Contour interval is 0.1.

may be different on the sphere. This deserves further exploration.

b. *Spatial structures of eddy-driven NAO patterns in a prespecified shifting jet, but with no topography*

To clearly see the impact of the meridional position of a prespecified shifting jet on the spatial structure of the NAO pattern, here we consider a prespecified shifting jet as shown in Fig. 1 and neglect the topographic effect. Under the same parameter condition as in Fig. 9 the streamfunction anomalies ψ_A of the eddy-driven negative-phase NAO pattern are shown in Fig. 10 for the northward ($\alpha_2 = -0.24$) and southward ($\alpha_2 = 0.24$) shifting jets. Figure 10 shows that in the absence of topography the eddy-driven negative-phase NAO dipole anomaly can exhibit a NE–SW (NW–SE) tilting only when the core of the prespecified jet has a northward (southward) excursion from a symmetric jet. However, the spatial tilting of the NAO pattern cannot occur in the absence of topography if the prespecified jet is symmetrical in the meridional direction (not shown). This result also holds for the positive NAO phase (not shown). Therefore, under the condition without topographic forcing the north–south excursion of the prespecified jet is extremely important for the spatial tilting of the eddy-driven NAO pattern. It is interesting to note that the eddy-driven NAO patterns look more like a propagating Rossby wave train in the presence of a shifting jet. Thus, in a westerly jet with a strong meridional excursion, the eddy-driven dipole anomaly easily exhibits a propagating Rossby wave train. This is easily seen in the Pacific basin where the basic westerly jet undergoes usually a strong north–south excursion during the El Niño–Southern Oscillation (ENSO) cycle.

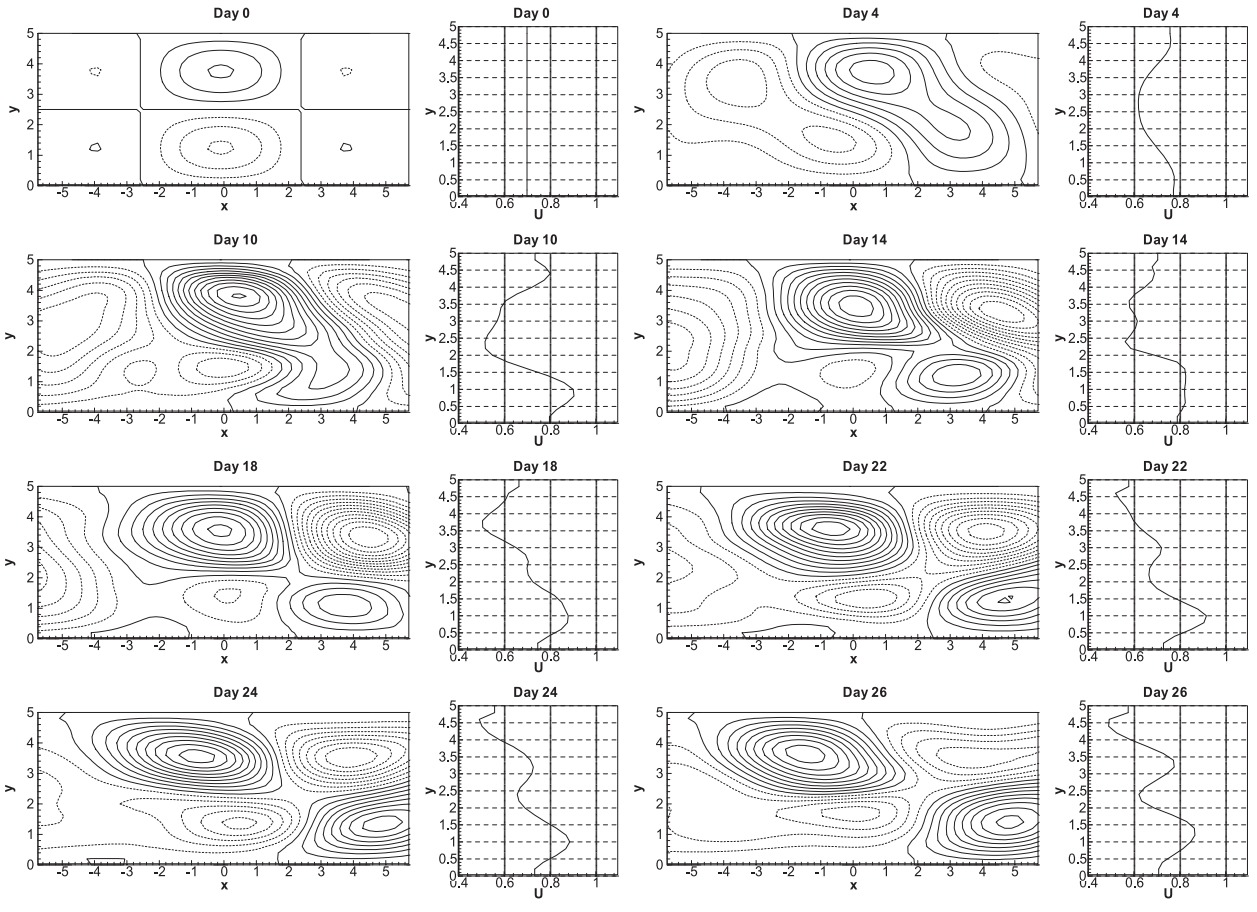

(b)

FIG. 11. (*Continued*)

c. *Spatial structures of eddy-driven NAO patterns in the presence of both a prespecified uniform westerly wind and topography*

Here we consider a case in which both topography and a prespecified uniform westerly wind ($\alpha_1 = 0$ and $\alpha_2 = 0$) are present. For the positive (negative) NAO phase, we choose the parameters $h_0 = -0.2$ and $m = 2\pi/L_y$ ($h_0 = 0.2$ and $m = -2\pi/L_y$) as an example. The instantaneous time sequences of the resulting streamfunction anomaly ψ_A of the eddy-driven NAO pattern and the time-dependent mean flow $U(y, t)$ are shown in Fig. 11 for the positive and negative phases.

It is found that a NAO dipole anomaly can be excited through the forcing of synoptic-scale waves in the presence of topography. Although the spatial tilting of the eddy-driven NAO pattern seems to depend on its phase, it is actually determined by the spatial distribution of the mean flow $U(y, t)$ associated with the NAO anomaly. For the positive phase the intensified jet is shifted to the north (Fig. 11a at day 14) so that the NAO dipole anomaly exhibits a northeast–southwest tilting. But such a spatial tilting tends to be weak once the intensified jet becomes symmetric in the meridional direction (Fig. 11a at days 22–26). For the negative phase, the NAO dipole anomaly can, however, show a marked northwest–southeast tilting in association with a southward shift of the intensified jet (Fig. 11b at days 22–26). As theoretically demonstrated by Luo et al. (2007b), in a prespecified uniform westerly wind the eddy-driven NAO dipole anomaly can drive a westerly jet to shift latitudinally through the interaction with the stationary topographic wave in the Atlantic basin, but the shift direction of the jet core is dominated by the phase of the NAO pattern. For the positive (negative) phase, the intensified jet is shifted to the north (south), resulting in a NE–SW (NW–SE) tilting in the latitudinal direction. The northward (southward) shift of the zonal mean flow during the positive (negative) phase NAO period is more prominent if the topographic height is increased

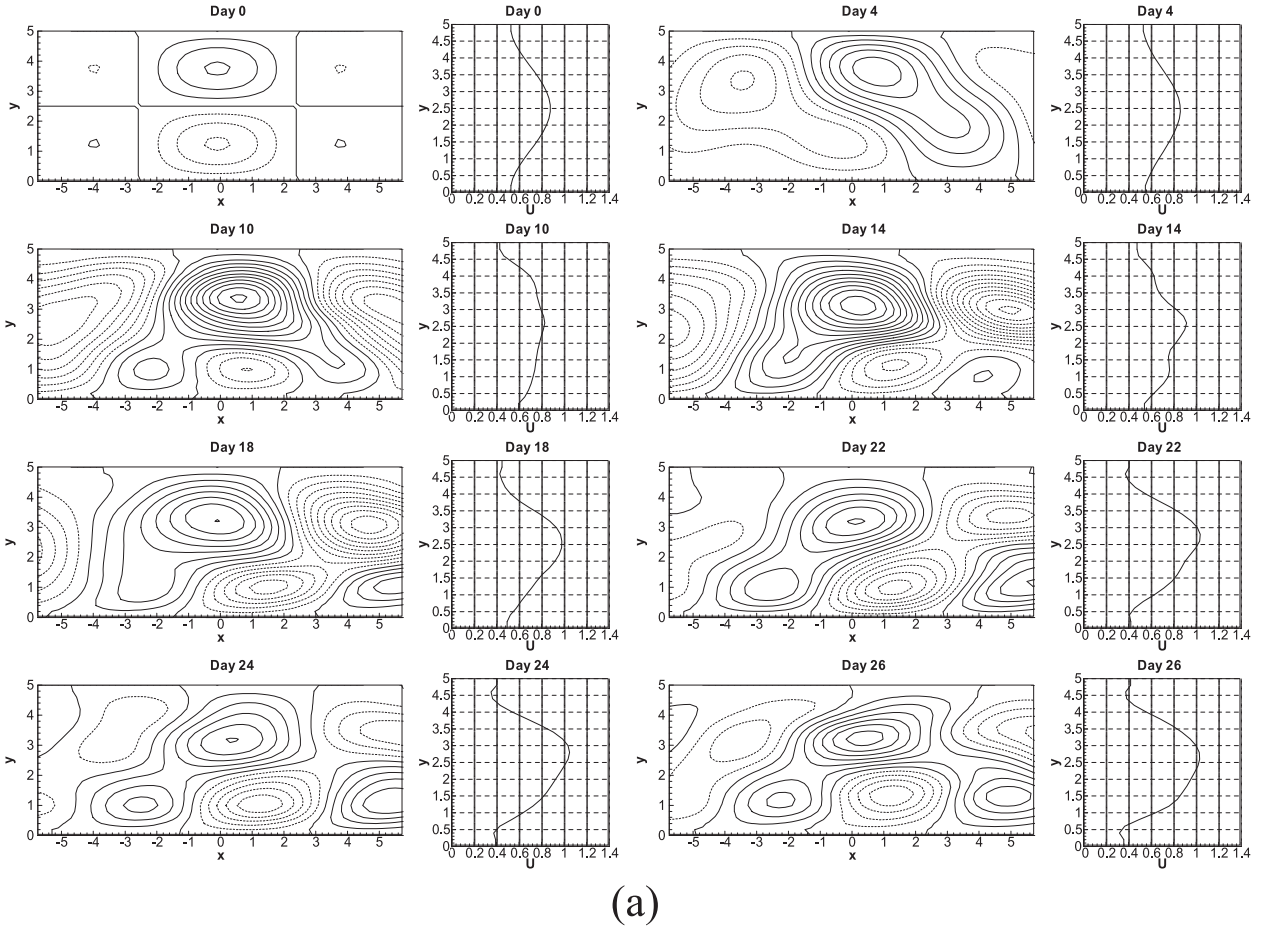

FIG. 12. Instantaneous time sequences of the streamfunction anomaly ψ_A and the time-dependent mean flow $U(y, t)$ of eddy-driven negative NAO phase patterns for three types of jets: (a) a symmetric jet ($\alpha_2 = 0$), (b) a northward-shifting jet ($\alpha_2 = -0.24$), and (c) a southward-shifting jet ($\alpha_2 = 0.24$). Contour interval is 0.1.

(not shown). In this case, the NE–SW (NW–SE) tilting of the positive (negative)-phase NAO pattern becomes more notable (not shown). In particular, in the presence of a strong topography wave anomalies develop easily downstream to form a wave train, which can resemble a Pacific–North America (PNA) pattern (Franzke et al. 2010, personal communication). Such a wave train can also be clearly seen in a shifting jet even if the topography is absent (Fig. 10). Thus, both the strong topography and shifting jet favor the excitation of propagating Rossby wave trains under the forcing of synoptic-scale waves. This is evident in the Pacific basin where the PNA is usually observed during the ENSO cycle. As shown in Fig. 9, the eddy-driven dipole pattern looks more like the observed NAO anomalies when the topography is absent and when the basic flow is both uniform and weak. Thus, it is likely that in our numerical model some of the eddy-driven patterns can resemble propagating wave trains due to the forcing of topography and the effect of a prespecified shifting jet. However, the eddy-driven NAO pattern in the numerical model can become the observed NAO pattern if the topography and the meridional shift of the prespecified westerly jet are relatively weak (not shown).

Another interesting point found from Figs. 11a and 11b is that the northward shift of the jet core for the positive phase seems to occur earlier than the southward shift of the jet core for the negative phase. This leads to the northeast–southwest tilting of the positive phase NAO pattern occurring earlier than the northwest–southeast tilting of the negative phase NAO pattern.

d. Spatial structures of the eddy-driven NAO with a prespecified shifting jet and topography

In this subsection, we will focus on how the spatial tilting of the eddy-driven NAO depends on the meridional shift of a prespecified jet in the presence of topography. To see this, a negative phase case is only

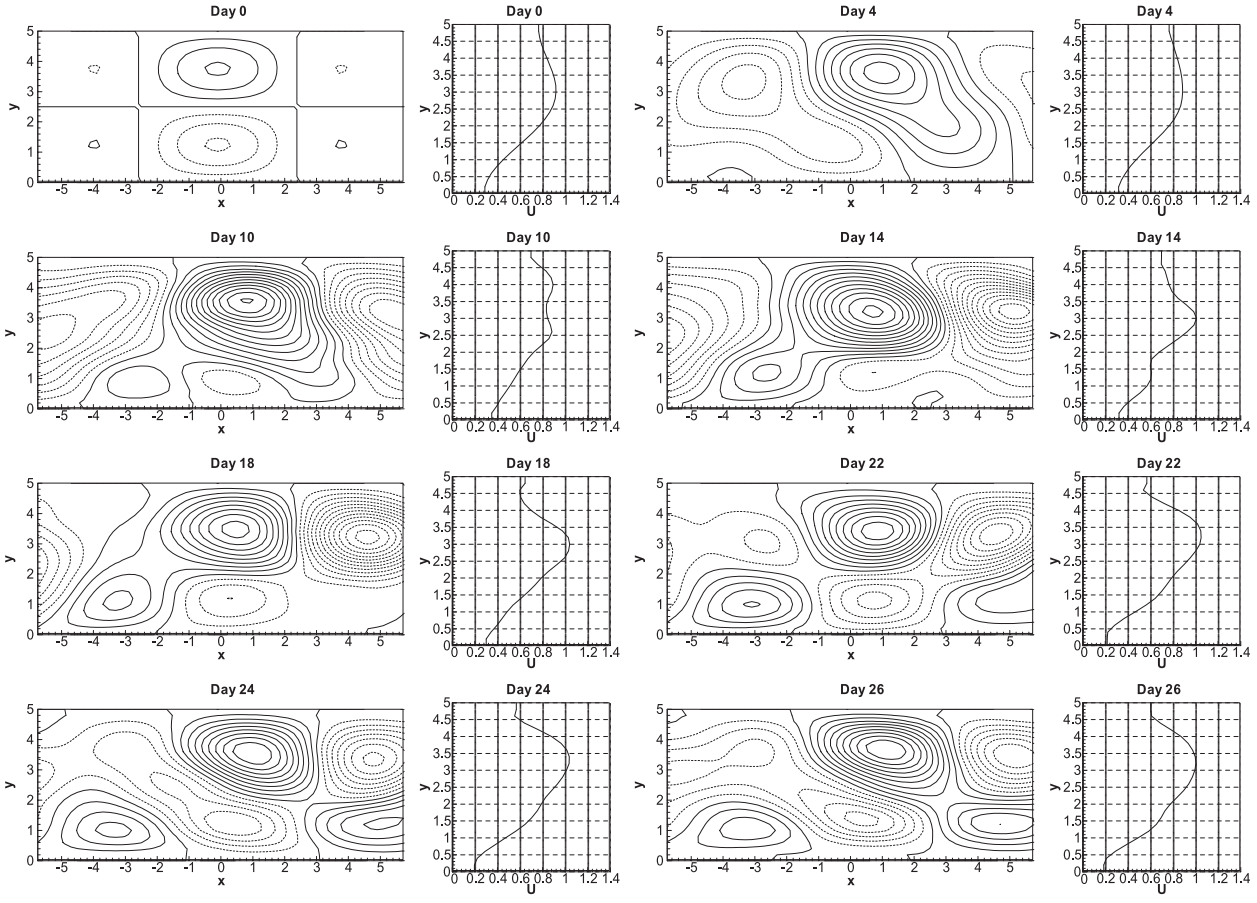

(b)

FIG. 12. (*Continued*)

considered here. The instantaneous time sequences of the streamfunction anomaly ψ_A and the time-dependent mean flow $U(y, t)$ of the eddy-driven negative phase NAO pattern are shown in Fig. 12 for three cases of a prescribed jet: $\alpha_2 = 0$, $\alpha_2 = -0.24$, and $\alpha_2 = 0.24$.

It is seen that for a prespecified symmetric jet ($\alpha_2 = 0$), the eddy-driven dipole anomaly can still display a NW–SE tilting due to the strong westerly winds in relatively low-latitude regions in the presence of topography (Fig. 12a). However, it shows a weak NE–SW tilting once the jet has a northward shift (Fig. 12b). A possible cause of this is that the southward-shifting jet produced by the interaction between the negative-phase NAO dipole anomaly and a stationary (topographic) wave will partly counteract the northward shift of the prespecified jet so that the eddy-driven negative phase NAO anomaly undergoes a weak NE–SW tilting (Fig. 12b). This NAO anomaly can also show a NW–SE tilting if the northward shift of the time-dependent mean flow exceeds that of this prespecified jet (not shown). Thus, the northward displacement of a prespecified jet tends to suppress the NW–SE tilting of the negative phase NAO pattern; even the NAO pattern can show a weak NE–SW tilting. If the core of the prespecified jet is within lower latitudes, the eddy-driven NAO dipole anomaly can display a distinct NW–SE tilting (Fig. 12c). This is because the southward-shifting jet produced by the interaction between the amplified negative-phase dipole anomaly and a stationary topographic wave can enhance the southward shift of the prescribed jet so that the NAO-induced jet is notably intensified in the lower-latitude region. In this case, the amplified NAO dipole anomaly propagates eastward more rapidly in the lower latitudes than in the higher latitudes, thus resulting in a marked NW–SE tilting. A similar result can also be found for the positive phase (not shown). On the other hand, we can find that, when the prespecified jet has a stronger northward (southward) shift, the positive phase (negative phase)

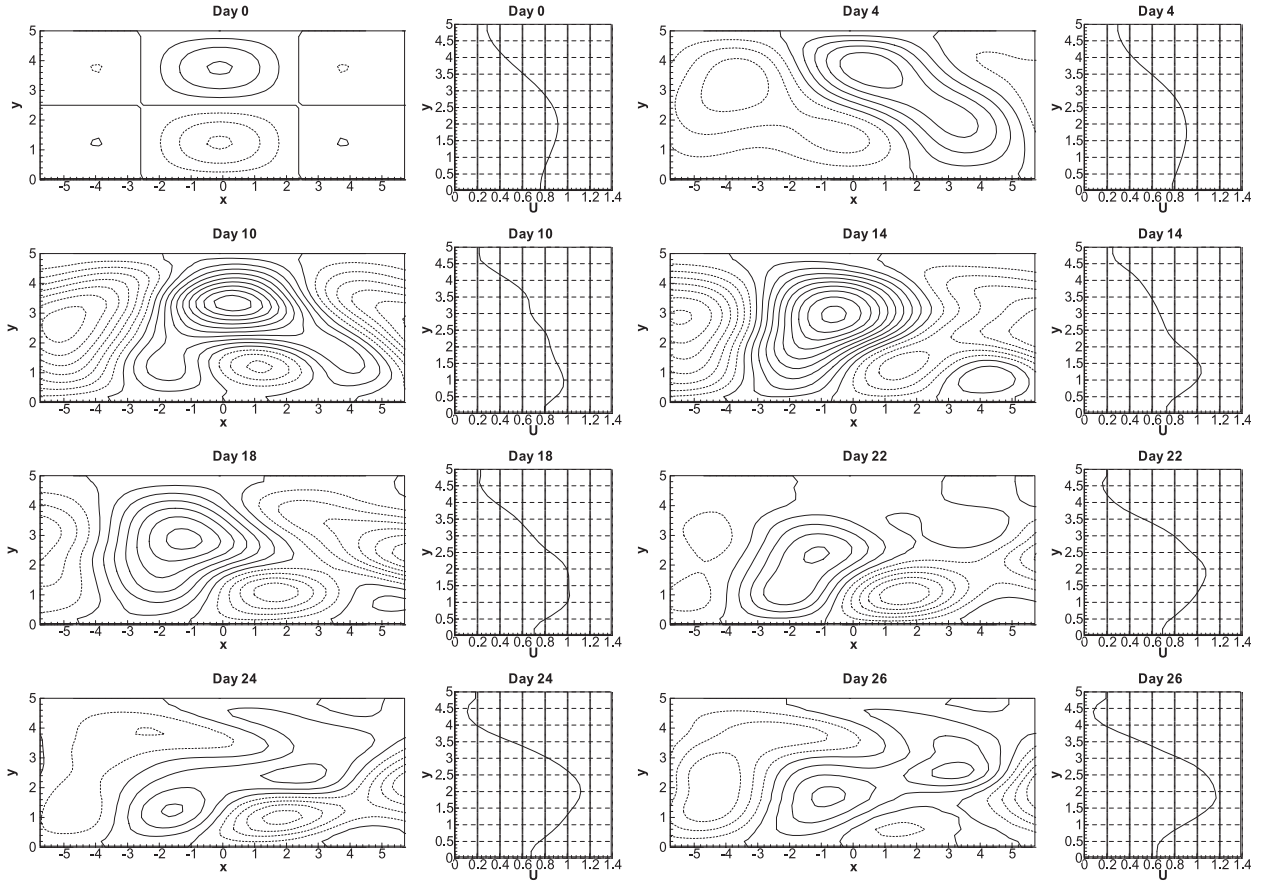

(c)

FIG. 12. (*Continued*)

NAO pattern can exhibit a more distinct NE–SW (NW–SE) tilting (not shown). It is worth pointing out that the eddy-driven dipole anomaly can exhibit propagating Rossby wave trains through the energy dispersion in the presence of a strong shifting jet or strong topography (Figs. 10–12). The relationship between the latitudinal distribution of the time-dependent mean flow and spatial tilting of the NAO found in Part I still holds even though the eddy-driven dipole pattern does not strictly resemble the observed NAO anomaly. The NAO pattern obtained from our numerical model shows a weak similarity to the composite NAO pattern (Figs. 2 and 3 in Part I), which may be due to the inclusion of the stationary wave anomaly component induced by the topography and the choice of the highly idealized basic flow before a NAO event occurs.

The above numerical experiments seem to indicate that the spatial tilting of the eddy-driven NAO anomaly is affected not only by the meridional excursion of the prespecified jet but also by the presence of topography. In particular, in the presence of topography, the spatial tilting of the eddy-driven NAO pattern can become dependent on its phase because the latitudinal distribution of the time-dependent mean flow is different for different phases of the NAO. This result also holds for other parameters (not shown).

5. Impact of the longitudinal position of the synoptic-scale wavemaker on the eddy-driven NAO pattern

a. Effect of the synoptic-scale wavemaker position on the spatial tilting of the eddy-driven NAO pattern

The instantaneous time sequences of the planetary-scale anomalies ψ_A and the time-dependent mean flow $U(y, t)$ of eddy-driven positive-phase NAO events for synoptic-scale wavemakers with different positions with $x_s = 1$ and $x_s = 3$ are shown in Fig. 13 for the positive

phase with both a prespecified northward-shifting jet and topography. In the presence of topography the northeast–southwest tilting of the eddy-driven NAO pattern for the positive phase is more distinct for $x_s = 1$ than for $x_s = 3$, which is particularly distinct during the period from days 16 to 28. A similar conclusion is also found for the negative phase (not shown).

The corresponding mean fields during the period from days 16 to 28 are also shown in Fig. 14. It is found that in a mean sense the positive NAO phase pattern does, indeed, show a more notable NE–SW tilting for $x_s = 1$ than for $x_s = 3$. That is, when the Atlantic storm-track eddy activity undergoes an eastward shift, the eddy-driven NAO pattern can show a more notable NE–SW tilting, which provides a likely explanation for why the first empirical orthogonal function (EOF) NAO pattern exhibits a more distinct NE–SW tilting during P3 than during P2 (see Fig. 1 of Part I). This is because when the Atlantic storm-track eddy activity is located farther east, for example during P3 (see Fig. 7 of Part I), the amplitude of the eddy-driven NAO becomes stronger so that the NAO-induced jet can exhibit a prominent northward shift even though the duration of the NAO may be relatively short. Thus, it is inevitable that the NAO pattern can exhibit a pronounced NE–SW tilting during P3. In this case, it is concluded that the zonal position of the Atlantic storm-track eddy activity is also an important factor for the spatial tilting of the NAO pattern.

b. *A link between the longitudinal position of the synoptic-scale wavemaker and the zonal shift of eddy-driven NAO patterns*

To confirm whether the whole eastward shift of the eddy-driven NAO anomaly is induced by the eastward shift of the Atlantic storm-track eddy activity (Part I), we design five experiments here to investigate a possible relationship between the zonal position of the synoptic-scale wavemaker and the whole shift of the eddy-driven NAO anomaly in the zonal direction. These numerical experiments are detailed in Table 1. For the positive and negative phases, the dependence of the zonal position of the eddy-driven NAO anomaly on the distance D_s of the synoptic-scale wavemaker relative to the initial NAO center is shown in Fig. 15.

It is seen that for two phases of the NAO the longitudinal location of the eddy-driven NAO anomaly seems to be dominated by the position of the synoptic-scale wavemaker, which also holds for other experiments. Although the details of the results of these control experiments are slightly different, it is certain that, when the wavemaker is located more westward, the center of action of the eddy-driven NAO for its two phases is displaced farther westward (Figs. 15a,b). In other words, the center of the NAO action is displaced farther eastward when the wavemaker is located farther eastward. We also find that widening the wavemaker does not affect the eastward shift of the NAO pattern (not shown). Thus, it is reasonable to infer that the position of the center of action of the NAO pattern is dominated by the zonal location of the Atlantic storm-track eddy activity. When the Atlantic storm-track eddy activity exhibits an eastward displacement, the eddy-driven NAO pattern can show an eastward shift. This confirms the result of Part I that the eastward shift of the center of the NAO pattern during P2 is closely related to the eastward displacement of the Atlantic storm-track eddy activity, in contrast to the finding of Jung et al. (2003) that the eastward shift of the North Atlantic cyclone activity results from the eastward shift of the centers of action of the NAO patterns. The GCM experiments also confirmed that the teleconnection patterns (NAO and PNA anomalies) are determined by the zonal positioning of storm tracks (Franzke et al. 2000, 2001). Actually, it is difficult to determine the cause and effect for the NAO pattern and the Atlantic storm-track eddy activity from observations because both the NAO pattern and the storm-track eddy activity are coupled together. Even so, there is no contradiction between the two viewpoints. This is because the climatological position of the eddy-driven NAO pattern in the zonal direction is dominated by the zonal position of the climatological Atlantic storm-track eddy activity, while the intensified NAO pattern for each NAO event can reorganize the Atlantic storm track and will determine its final position during its life cycle (Luo et al. 2007a). Thus, in a climatological sense the zonal position of the Atlantic storm-track eddy activity is a key factor for the existing region of the NAO anomaly.

TABLE 1. The five experiments of the eddy-driven NAO anomalies for different background flows and topography. Experiment 1 (expt 1) represents the case in which the background flow prior to NAO onset is uniform and the topography is present. Experiment 2 (expt 2) refers to the case in which the background flow prior to NAO onset is uniform and the topography is absent. Experiment 3 (expt 3) refers to the case in which the prescribed jet is symmetric in the meridional direction and the topography is absent. Experiments 4 and 5 (expts 4 and 5) represent that the prescribed jet is shifted to the south and north respectively, but no topography is included in the two experiments. Here the presence of topography is referred to as "Yes" and the absence of topography is referred to as "No".

Expt 1	Yes	Uniform westerly wind
Expt 2	No	Uniform westerly wind
Expt 3	No	Symmetric jet
Expt 4	No	Southward-shifting jet
Expt 5	No	Northward-shifting jet

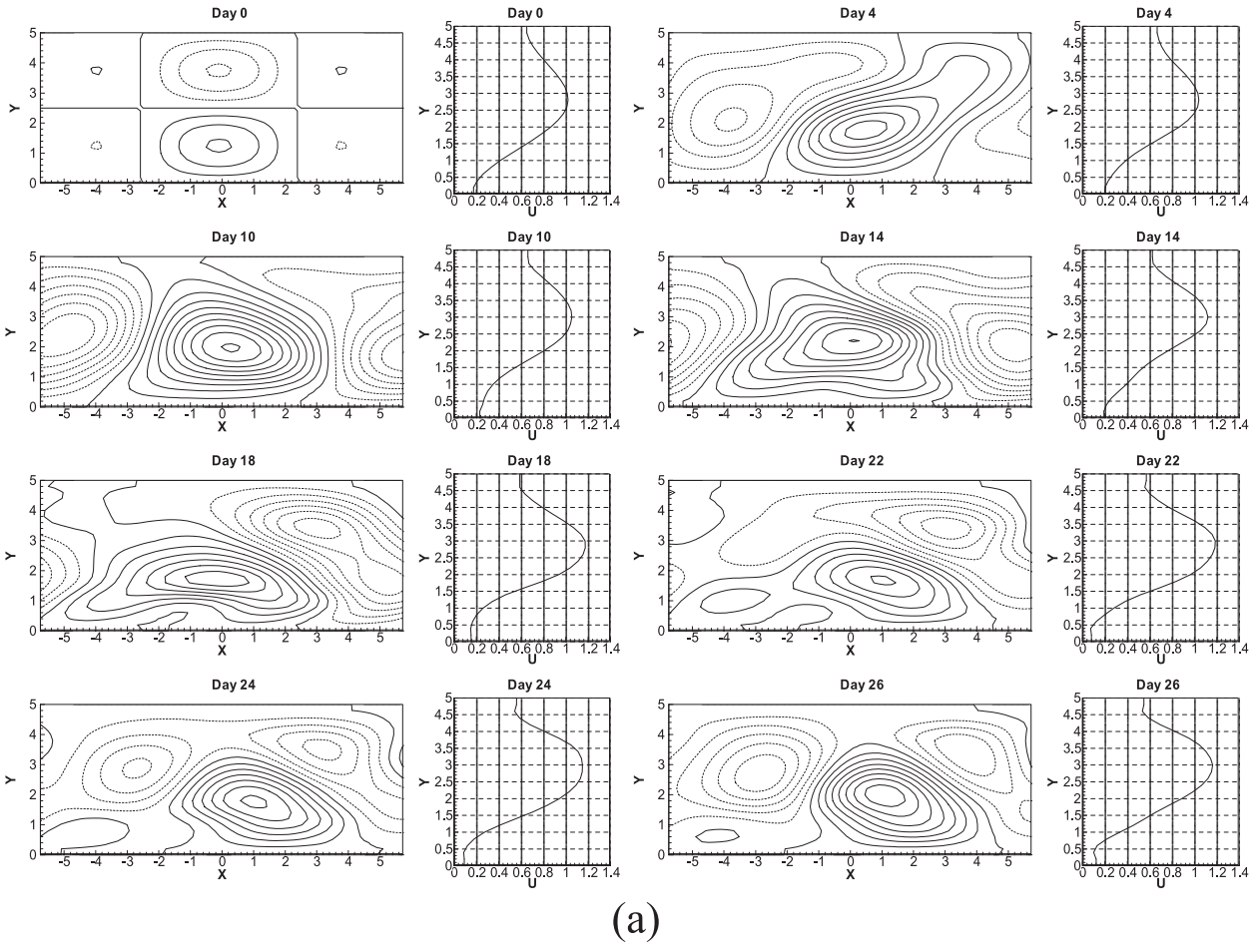

FIG. 13. Instantaneous time sequences of the streamfunction anomaly ψ_A and the time-dependent mean flow $U(y, t)$ of the eddy-driven positive NAO phase pattern in a northward-shifting jet and with topography for the wavemakers with different positions of (a) $x_s = 1$ and (b) $x_s = 3$. Contour interval is 0.1.

6. Conclusions and discussion

In the present paper, the numerical solutions of linear and nonlinear models without forcing are first presented to demonstrate that the meridional distribution of the prior basic flow is important for the subsequent spatial structure of a dipole Rossby anomaly. For this case, the spatial tilting of the dipole structure is independent of the NAO's phase. When the core of a prescribed jet is in the higher (lower) latitudes, the subsequent dipole anomaly shows a NE–SW (NW–SE) tilting regardless of its phase. In a fully nonlinear experiment with a wavemaker that mimics the Atlantic storm-track eddy activity but without topography, the spatial tilting of the NAO pattern is also found to be independent of the NAO phase. For both positive and negative phases the eddy-driven NAO pattern can show a NE–SW (NW–SE) tilting as the prespecified jet prior to the NAO undergoes a northward (southward) excursion, but becomes almost symmetric in the meridional direction once the jet is a symmetric jet. However, in the presence of the wavenumber-2 topography (two oceans and continents) the spatial tilting of the eddy-driven NAO pattern becomes dependent on the NAO phase. The NAO pattern can exhibit a NE–SW (NW–SE) tilting for the positive (negative) phase in the presence of topography even though the prespecified basic flow may be a uniform westerly wind or a symmetric jet. This is because an intensified northward (southward) shifting jet can be formed for the positive (negative) NAO phase in the presence of topography and then can determine the tilting direction of the NAO pattern.

In addition, it is found that the NE–SW (NW–SE) tilting of the NAO pattern for the positive (negative) phase becomes more notable once the Atlantic jet prior to the NAO has a more distinct northward (southward)

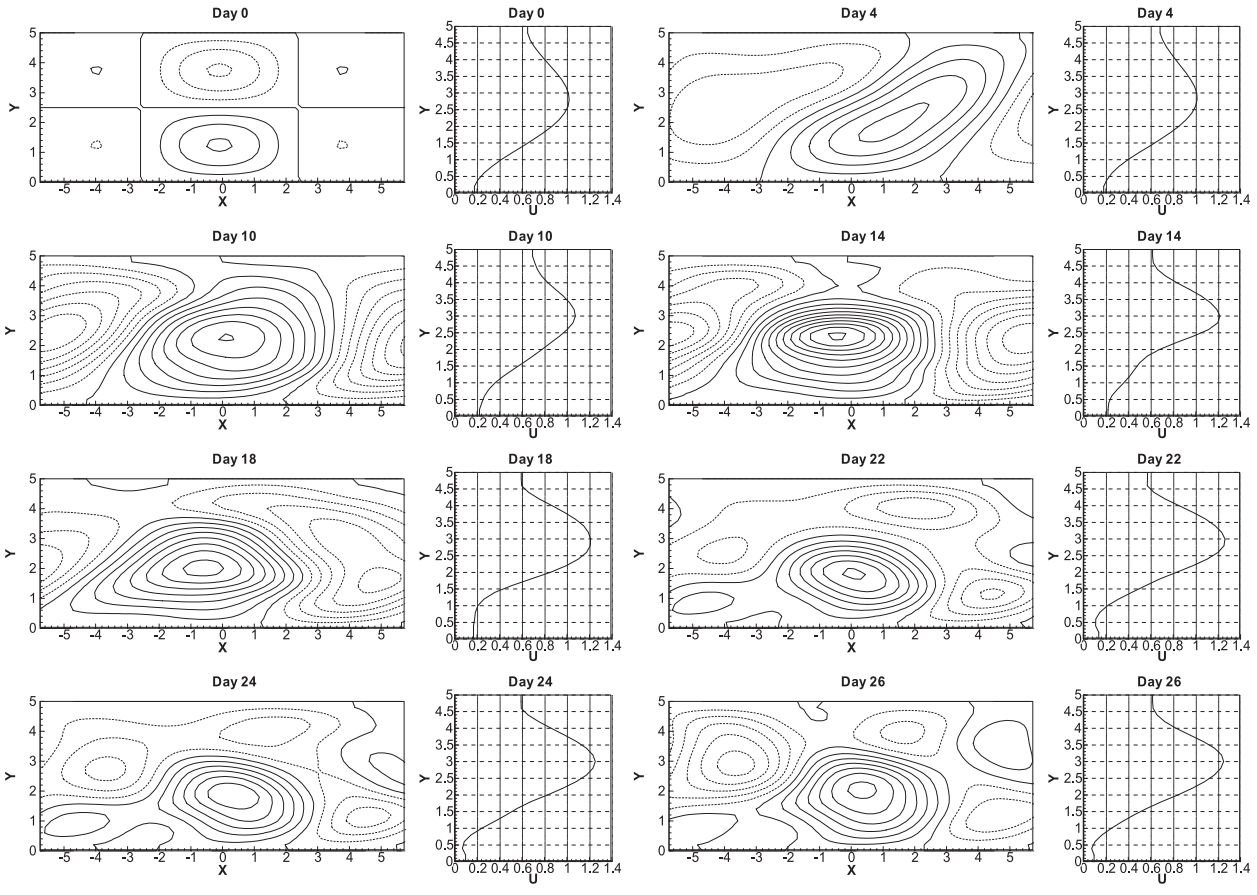

(b)

FIG. 13. (*Continued*)

excursion. In particular, we find that, in the presence of the strong topography or a prespecified shifting jet, the eddy-driven planetary-scale pattern evolves easily into a propagating Rossby wave train. This is seen in the Pacific basin where the topographic forcing and the effect of the shifting jet play an important role for the PNA (Franzke et al. 2010, personal communication). For example, during the ENSO cycle the meridional displacement of the Pacific jet is rather pronounced so the eddy-driven pattern can have a Rossby wave train like the PNA.

It is further shown that the zonal position of the wavemaker (Atlantic storm-track eddy activity) exerts an important influence on the spatial tilting and zonal shift of the eddy-driven NAO pattern. When the wavemaker is located farther eastward, the eddy-driven NAO pattern can show a more distinct NE–SW (NW–SE) tilting for the positive (negative) phase and a notable whole eastward shift, consistent with the observational results in Part I. In Part I it is shown that the first EOF NAO pattern has a more distinct northeast–southwest tilting during P3 than during P2 and the Atlantic storm-track eddy activity is located farther eastward during P3 than during P2.

A shortcoming of this paper is that the equivalent barotropic model used in the present paper cannot reflect the baroclinic synoptic-scale eddy activity in the Atlantic storm track and the vertical structure of the observed NAO dipole pattern. In spite of this, the barotropic model provides insight into the physical dynamics of why the NAO for different phases can have different spatial tilting and why the centers of action of the NAO pattern can show a whole eastward shift during P2 (P3) compared to the period of P1. Of course, the results here are based on a simple model; whether the results hold in more complex systems is also an interesting issue. Thus, an extension of the present numerical model to a baroclinic atmosphere is necessary. In addition, other factors such as the influence of sea surface temperature anomalies in the Atlantic basin and land–sea thermal contrast on the spatial tilting of the NAO

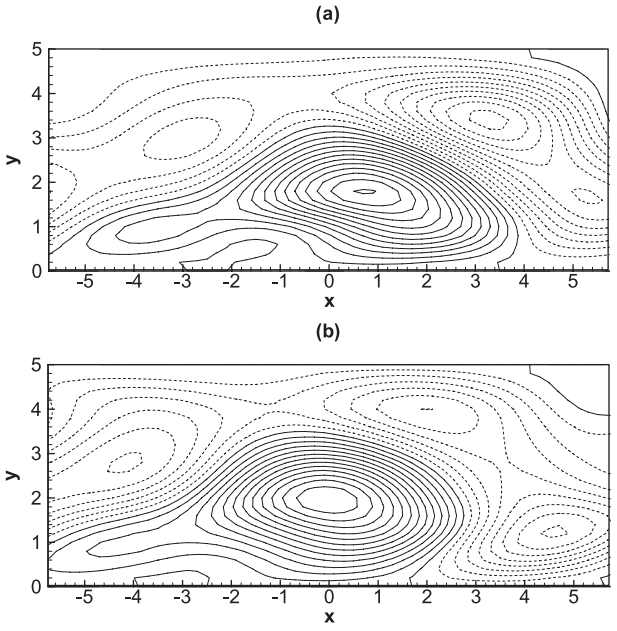

FIG. 14. Mean field from 16 to 28 days of the eddy-driven NAO anomaly: model parameters as in Fig. 13.

pattern are also excluded in the present model. These issues deserve further investigation.

Acknowledgments. The authors acknowledge the support from the National Science Foundation Innovation Group Program (40921004), Taishan Scholar funding, FANEDD, the Chinese Ministry of Education's 111 Project (B07036), and NSFC (40705016). We are also grateful to three anonymous reviewers for their constructive comments and suggestions.

REFERENCES

Arakawa, A., 1966: Computational design for long-term numerical integration of the equations of fluid motion: Two-dimensional incompressible flow. Part I. *J. Comput. Phys.,* **1,** 119–143.

Benedict, J. J., S. Lee, and S. B. Feldstein, 2004: Synoptic view of the North Atlantic Oscillation. *J. Atmos. Sci.,* **61,** 121–144.

Charney, J. G., and J. G. DeVore, 1979: Multiple flow equilibria in the atmosphere and blocking. *J. Atmos. Sci.,* **36,** 1205–1216.

Feldstein, S. B., 2003: The dynamics of NAO teleconnection pattern growth and decay. *Quart. J. Roy. Meteor. Soc.,* **129,** 901–924.

Franzke, C., K. Fraedrich, and F. Lunkeit, 2000: Low-frequency variability in a simplified atmospheric global circulation model: Storm-track induced "spatial resonance". *Quart. J. Roy. Meteor. Soc.,* **126,** 2691–2708.

——, ——, and ——, 2001: Teleconnections and low-frequency variability in idealized experiments with two storm tracks. *Quart. J. Roy. Meteor. Soc.,* **127,** 1321–1339.

——, S. Lee, and S. B. Feldstein, 2004: Is the North Atlantic Oscillation a breaking wave? *J. Atmos. Sci.,* **61,** 145–160.

Hilmer, M., and T. Jung, 2000: Evidence for a recent change in the link between the North Atlantic Oscillation and Arctic sea ice export. *Geophys. Res. Lett.,* **27,** 989–992.

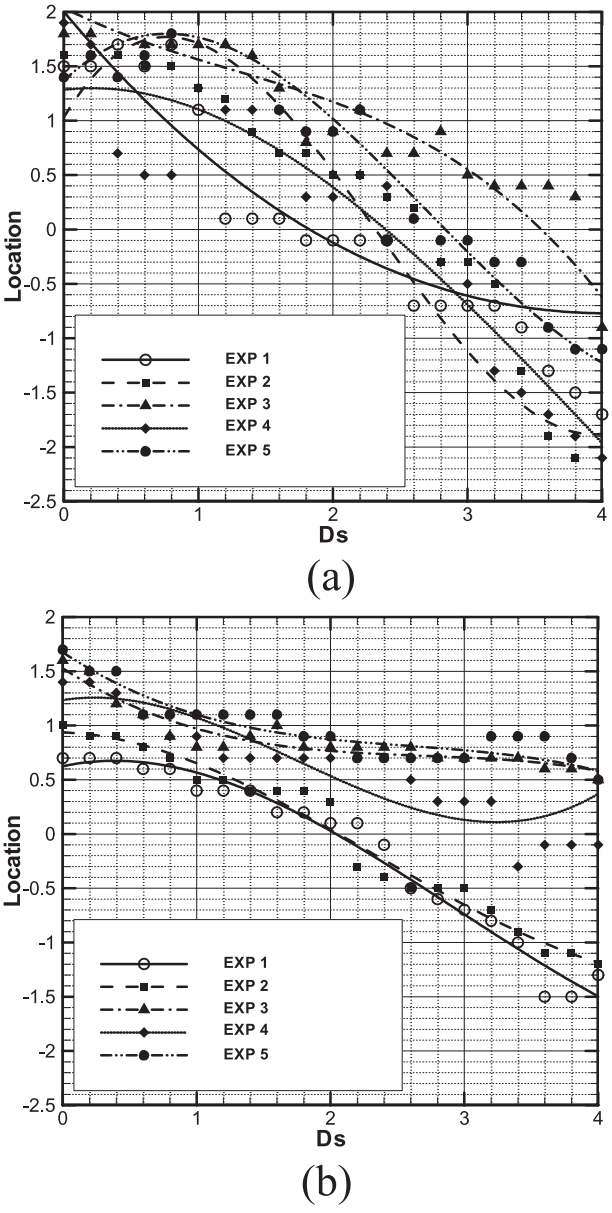

FIG. 15. Dependence of the zonal position of the eddy-driven NAO anomaly on the distance D_s of the synoptic-scale wavemaker relative to the initial NAO center for five control experiments listed in Table 1 for the (a) positive and (b) negative NAO phases.

Holland, W. R., and L. B. Lin, 1975: On the generation of mesoscale eddies and their contribution to the oceanic general circulation. I. A preliminary numerical experiment. *J. Phys. Oceanogr.,* **5,** 642–657.

Hurrell, J. W., 1995: Decadal trends in the North Atlantic Oscillation: Regional temperature and precipitation. *Science,* **269,** 676–679.

Johnson, N. C., S. B. Feldstein, and B. Trembley, 2008: The continuum of Northern Hemisphere teleconnection patterns and a description of the NAO shift with the use of self-organizing maps. *J. Climate,* **21,** 6354–6371.

Jung, T., and M. Hilmer, 2001: The link between the North Atlantic Oscillation and Arctic sea ice export through Fram Strait. *J. Climate,* **14,** 3932–3943.

——, ——, E. Ruprecht, S. Kleppek, S. K. Gulev, and O. Zolina, 2003: Characteristics of the recent eastward shift of interannual NAO variability. *J. Climate,* **16,** 3371–3382.

Luo, D., 2005: A barotropic envelope Rossby soliton model for block–eddy interaction. Part I: Effect of topography. *J. Atmos. Sci.,* **62,** 5–21.

——, and T. Gong, 2006: A possible mechanism for the eastward shift of interannual NAO action centers in last three decades. *Geophys. Res. Lett.,* **33,** L24815, doi:10.1029/2006GL027860.

——, A. Lupo, and H. Wan, 2007a: Dynamics of eddy-driven low-frequency dipole modes. Part I: A simple model of North Atlantic Oscillations. *J. Atmos. Sci.,* **64,** 3–38.

——, T. Gong, and Y. Diao, 2007b: Dynamics of eddy-driven low-frequency dipole modes. Part III: Meridional displacement of westerly jet anomalies during two phases of NAO. *J. Atmos. Sci.,* **64,** 3232–3248.

——, ——, and L. Zhong, 2008: Dynamical relationship between the phase of North Atlantic Oscillations and meridional excursion of a preexisting jet: An analytical study. *J. Atmos. Sci.,* **65,** 1838–1858.

——, Z. Zhu, R. Ren, L. Zhong, and C. Wang, 2010: Spatial pattern and zonal shift of the North Atlantic Oscillation. Part I: A dynamical interpretation. *J. Atmos. Sci.,* **67,** 2805–2826.

Peterson, K. A., J. Lu, and R. J. Greatbatch, 2003: Evidence of nonlinear dynamics in the eastward shift of the NAO. *Geophys. Res. Lett.,* **30,** 1030, doi:10.1029/2002GL015585.

Shutts, G. J., 1983: The propagation of eddies in diffluent jet streams: Eddy vorticity forcing of blocking flow fields. *Quart. J. Roy. Meteor. Soc.,* **109,** 737–761.

Ulbrich, U., and M. Christoph, 1999: A shift of the NAO and increasing storm track activity over Europe due to anthropogenic greenhouse gas forcing. *Climate Dyn.,* **15,** 551–559.

Woollings, T. J., B. J. Hoskins, M. Blackburn, and P. Berrisford, 2008: A new Rossby wave-breaking interpretation of the North Atlantic Oscillation. *J. Atmos. Sci.,* **65,** 609–626.